NAVAL POSTGRADUATE SCHOOL

MONTEREY, CALIFORNIA

THESIS

DESIGN OF A MAXIMUM POWER POINT TRACKER WITH SIMULATION, ANALYSIS, AND COMPARISON OF ALGORITHMS

by

Jeff Wurz

December 2012

Thesis Advisor:	Robert Ashton
Second Reader:	Vladimir Dobrokhodov

THIS PAGE INTENTIONALLY LEFT BLANK

REPORT DOCUMENTATION PAGE

Form Approved
OMB No. 0704–0188

1. REPORT DATE *(DD–MM–YYYY)*	2. REPORT TYPE	3. DATES COVERED *(From — To)*
12–12–2012	Master's Thesis	2012-10-01—2012-12-31

4. TITLE AND SUBTITLE

Design of a Maximum Power Point Tracker with Simulation, Analysis, and Comparison of Algorithms

5a. CONTRACT NUMBER

5b. GRANT NUMBER

5c. PROGRAM ELEMENT NUMBER

6. AUTHOR(S)

Jeff Wurz

5d. PROJECT NUMBER

5e. TASK NUMBER

5f. WORK UNIT NUMBER

7. PERFORMING ORGANIZATION NAME(S) AND ADDRESS(ES)

Naval Postgraduate School
Monterey, CA 93943

8. PERFORMING ORGANIZATION REPORT NUMBER

9. SPONSORING / MONITORING AGENCY NAME(S) AND ADDRESS(ES)

Department of the Navy

10. SPONSOR/MONITOR'S ACRONYM(S)

11. SPONSOR/MONITOR'S REPORT NUMBER(S)

12. DISTRIBUTION / AVAILABILITY STATEMENT

Approved for public release; distribution is unlimited

13. SUPPLEMENTARY NOTES

The views expressed in this thesis are those of the author and do not reflect the official policy or position of the Department of Defense or the U.S. Government. IRB Protocol Number: N/A

14. ABSTRACT

In this thesis, the advantages of three different maximum power point tracking ($MPPT$) algorithm are investigated. By simulation, the performance and efficiency of these algorithms was analyzed. By using MATLAB's SimPowerSystems block set, we created the model comprised of a Kyocera KD135GX-LP solar panel powering a buck converter controlled by the $MPPT$ algorithms driving a resistive load. The main objective was to track the maximum power point (MPP) of the solar array by modulating the buck converter's duty cycle, thereby, optimizing the power output of the panel. The three algorithms observed performance was on par with other real world tests of these algorithms as seen in other published work. The Perturb and Observe ($P\&O$) algorithm performed with a higher overall efficiency and was able to track the MPP quickly, while the Incremental Conductance (InC) algorithm had similar performance but requires more intensive calculations. The analysis of these algorithms led to a greater understanding of where the inefficiencies of this type of system are located, allowing improvement in future work on this subject.

15. SUBJECT TERMS

MPPT, Maximum power point tracker, buck converter, solar array, simulation, MATLAB, incremental conductance, perturb and observe.

16. SECURITY CLASSIFICATION OF:			17. LIMITATION OF ABSTRACT	18. NUMBER OF PAGES	19a. NAME OF RESPONSIBLE PERSON
a. REPORT	b. ABSTRACT	c. THIS PAGE			19b. TELEPHONE NUMBER *(include area code)*
Unclassified	Unclassified	Unclassified	UU	113	

THIS PAGE INTENTIONALLY LEFT BLANK

Approved for public release; distribution is unlimited

DESIGN OF A MAXIMUM POWER POINT TRACKER WITH SIMULATION, ANALYSIS, AND COMPARISON OF ALGORITHMS

Jeff Wurz
Civilian, United States Navy
B.S., Electrical Engineering, University of California, Davis, 2008

Submitted in partial fulfillment of the
requirements for the degree of

MASTER OF SCIENCE IN ELECTRICAL ENGINEERING

from the

NAVAL POSTGRADUATE SCHOOL
December 2012

Author: Jeff Wurz

Approved by: Robert Ashton
Thesis Advisor

Vladimir Dobrokhodov
Second Reader

Clark Robertson
Chair, Department of Electrical Engineering

THIS PAGE INTENTIONALLY LEFT BLANK

ABSTRACT

In this thesis, the advantages of three different maximum power point tracking ($MPPT$) algorithm are investigated. By simulation, the performance and efficiency of these algorithms was analyzed. By using MATLAB's SimPowerSystems block set, we created the model comprised of a Kyocera KD135GX-LP solar panel powering a buck converter controlled by the $MPPT$ algorithms driving a resistive load. The main objective was to track the maximum power point (MPP) of the solar array by modulating the buck converter's duty cycle, thereby, optimizing the power output of the panel. The three algorithms observed performance was on par with other real world tests of these algorithms as seen in other published work. The Perturb and Observe ($P\&O$) algorithm performed with a higher overall efficiency and was able to track the MPP quickly, while the Incremental Conductance (InC) algorithm had similar performance but requires more intensive calculations. The analysis of these algorithms led to a greater understanding of where the inefficiencies of this type of system are located, allowing improvement in future work on this subject.

THIS PAGE INTENTIONALLY LEFT BLANK

Table of Contents

THIS PAGE INTENTIONALLY LEFT BLANK

List of Figures

List of Tables

THIS PAGE INTENTIONALLY LEFT BLANK

LIST OF ACRONYMS AND ABBREVIATIONS

CCM Continuous Conduction Mode
D Duty Cycle
DC Direct Current
InC Incremental Conductance
MPP Maximum Power Point
MPPT Maximum Power Point Tracker
NPS Naval Postgraduate School
P&O Perturb and Observe
PWM Pulse Width Modulation

THIS PAGE INTENTIONALLY LEFT BLANK

Executive Summary

The objective of this research was to investigate the improvements in solar power generation through use of a maximum power point tracker ($MPPT$) in conjunction with a buck converter. Solar energy is all around us during the day, the only problem is the inefficiency of current solar cells. Every year advances are made in the efficiency of solar cells, but overall the cells' greatest source of correctable inefficiency is in the implementation of the $MPPT$.

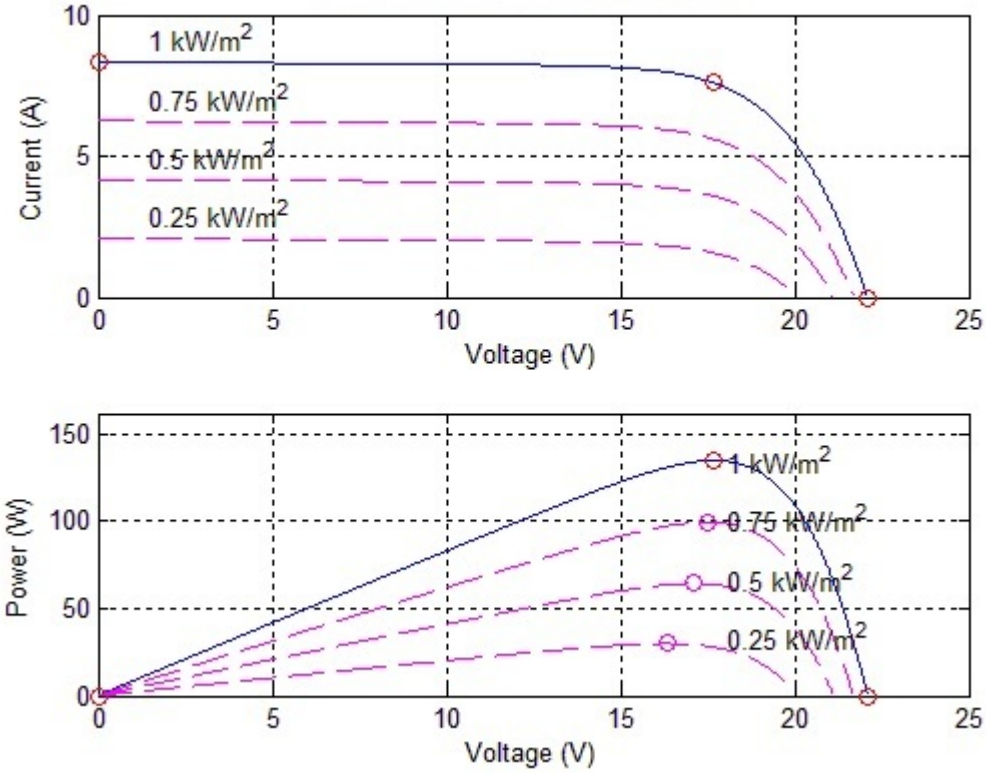

Figure 1: This is the Current versus Voltage and Power versus Voltage plots from the Kyocera KD135GX-LP panel modeled.

Solar cells operate as a reverse biased diode. Solar cells absorb light incident on their surface which recombines in the active region of the diode. In order to extract the most power from a solar cell, the equivalent resistance which allows the most voltage and current

output from the cell must be maintained. The maximum power point (*MPP*) can vary depending on the magnitude of irradiance and the temperature of the solar cell as seen in Figure 1. The major differences in the algorithms which will search for the *MPP* are speed, overshoot, and tracking efficiency. These three parameters must be balanced in order to achieve optimal power transfer within the system.

The optimized solar cell output power flows into a bucking converter which has its set point determined by the *MPPT* algorithm. There are three specific *MPPT* algorithms which were investigated: Perturb and Observe (*P&O*), Incremental Conductance (*InC*) and Constant Duty Cycle. By analyzing the output of these algorithms under different known conditions, the performance of each of these controllers was assessed. After generating the code necessary to implement these algorithms in the MATLAB environment, it was necessary to also construct an appropriate model using the SimPowerSystems block set to simulate the system, as seen in Figure 2.

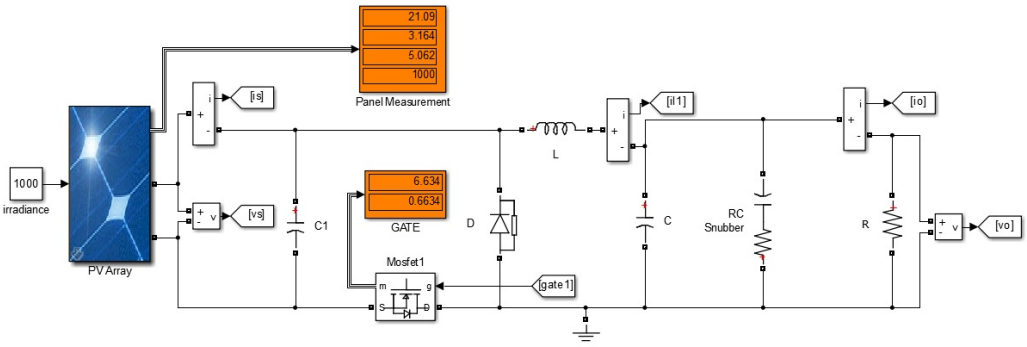

Figure 2: This figure shows the functional portion of the model under test in Simulink, which includes the solar array, buck converter, and resistive load.

The major differences in the algorithms which search for the *MPP* are speed, overshoot, and tracking efficiency. These three parameters must be balanced in order to achieve an optimal system.

The control of a bucking converter is achieved by modulating the duration the switch is 'on' or 'off' as seen in Figure 3. Essentially, the MOSFET switch controls the power flow, while the output low pass *LC* filter removes the switch discontinuity. Through control of the duty cycle (*D*), the output voltage is equal to the input voltage divided by *D*. Tuning the output filter reduces the output voltage ripple to an acceptable level.

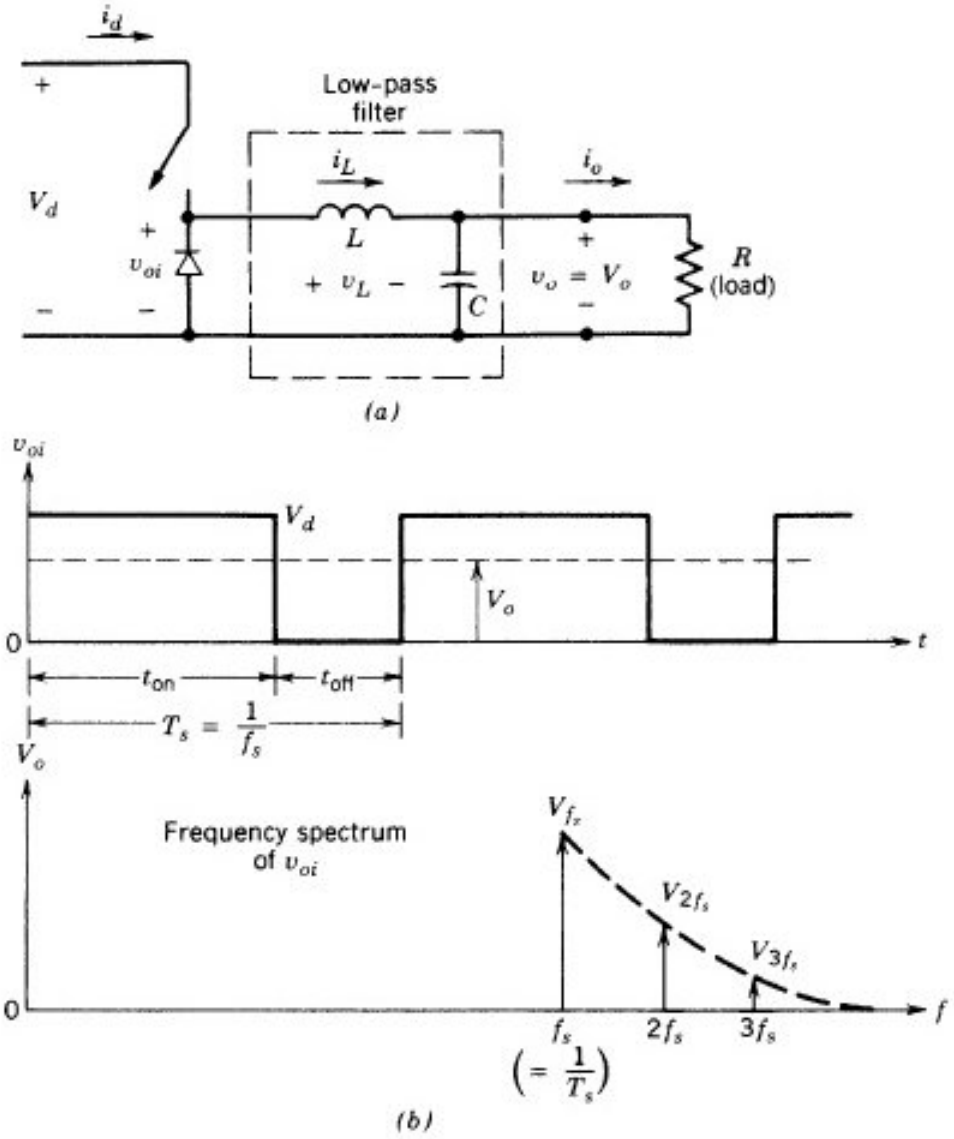

Figure 3: Bucking DC-DC converter showing simple circuit diagram (a), output voltage and frequency spectrum of output (b).

The comparison of the *MPPT* algorithms was a worthwhile endeavor. This simulation allowed for optimizations to be made prior to purchasing components or building a physical circuit. Pending future work, this effort may have great impact on solar powered unmanned air vehicles (*UAV*).

By optimizing the buck converter independent of the *MPPT* and the solar array, the efficiency of the converter was greater than 94% during steady state operation. This makes the conversion from the solar array quite efficient and attractive.

The ability to track the *MPP* further optimized the low efficiency solar array output. Since the solar array is the source of power to the system, any improvement in the ability to track the *MPP* similarly improves the overall system performance.

The actual data gathering runs were done in three parts. The first part included the *P&O* algorithm with constant $1000\,W/m^2$ Irradiance, a step in irradiance from $600\,W/m^2$ to $1000\,W/m^2$ at $0.08\,s$ to $0.01\,s$, and a random changing of irradiance to the solar array. Next, the constant D controller was used as well with the same three input signals. The constant D was used as the reference for comparison with the other algorithms. Finally, the *InC* algorithm was tested; although, the tuning of the parameters for this algorithm was the most difficult. The algorithm leads to either a very fast response to transients or undershoots the *MPP*. Because of the difficulty optimizing and the amount of time required to actually run each test, the *InC* algorithm was not optimized to match the performance of the *P&O* algorithm.

An innovation in the *P&O* algorithm was to include a two stage change in D in order to converge quickly to the target, yet still have fine granularity when approaching the *MPP*. This was not very difficult to implement and overall provided very fast tracking and convergence to the *MPP*. In the Appendix, the code used for this algorithm is provided. It

can be seen that with a multistage *MPPT*, the overall speed of the system remains fast and tracks the *MPP* well. Since this is not division, the operation does not require many extra calculation cycles to complete.

Overall, the expected outcome of the *P&O* algorithm was quite good. Since the algorithm can be optimized to meet certain timing requirements, it responded faster and performed better than the *InC* algorithm. This can only be accounted for due to the complexities of the *InC* algorithm computations and speed of operation. Due to the difficulty in optimizing the *InC* algorithm, the results from those runs do not accurately tell us the optimal operation of the algorithm. Given more time to properly optimize ΔD, the algorithm should have tracked the MPP quicker and with more certainty than the *P&O* algorithm.

THIS PAGE INTENTIONALLY LEFT BLANK

Acknowledgements

I would like to first and foremost thank the universe for existing.

Secondly, my advisor, Robert Ashton, who helped greatly with my limited time to complete this thesis.

I appreciated all those who reviewed my thesis prior to completion. Sue Hawthorne and Vladimir Dobrokhodov – without their help I am not sure any of this would have been possible.

My thanks also extend to my parents, Suzan and James Wurz, who dealt with my temporary insanity quite well.

THIS PAGE INTENTIONALLY LEFT BLANK

CHAPTER 1:

INTRODUCTION

It is a warm summer day. You feel the sun warm your skin and rejuvenate your motivation. The sun generates more energy than anything else in the solar system, but due to our distance from this writhing fireball, we are perfectly comfortable and able to sustain life. Life has figured out a way to harness this power emanating from 93 million miles away. By harnessing this power that is available all around us, we enable ourselves to free our bodies from the toils we once endured not 40 years ago. More and more automation is taking over our lives, and to power that automation we require a source of energy that will not be going away anytime soon, the perfect example of this being our sun. Without the sun, life would cease to be and, therefore, why not harness the sun to create a better life for those around to live it?

1.1 Objectives

The objective of this thesis is to determine the most cost effective and efficient method for maximum power point tracking ($MPPT$). Many optimizations can be done to a system. Knowing which will bring about the greatest change is truly the challenge.

Since fossil fuels are detrimental to the environment and also non-renewable, there has been an upsurge of interest in clean and renewable energy. While more than one option is available to fill that void, the most interesting and widespread so far is photovoltaics. Photovoltaics are semiconductor devices which convert solar irradiation in the visible spectrum to generate direct current (DC). With recent advances in technology and discoveries of new materials, solar cells are increasing in efficiency and flexibility. This change in what solar

panels are composed of has greatly increased the applications of these panels. The surface they are supported on no longer needs to be rigid and planar, and due to this they are now able to be used in applications that previously could not use photovoltaics.

In order to fully harness the power of the sun, we need to optimize the output from the solar panels. In the simplest terms a solar panel is a current source when short circuited and has a voltage while in open circuit configuration. The key to attaining the greatest output from the panels is to maintain an output impedance so that the solar panels operate at a point that corresponds to its maximum power point (MPP). The MPP is the operating point required to optimize the output power of the panels. Depending on weather conditions, the output power is proportional to the amount of incident light on the surface of the photovoltaics, as well as being inversely proportional to the temperature of the panels. This means that the hotter the panels get the less current they can provide at the output.

In order to convert the power from the solar array, we require a power converter that will be able to extract the most power from the array. By connecting a buck converter to the output of the solar array, we are then able to control the voltage of the solar array by varying the duty cycle (D) of the buck converter. When one is changing D, we want the voltage and current to provide the most power at a specific voltage level. In order to reach this voltage level, a control algorithm is implemented to track and follow the highest input power from the solar array. When this algorithm is functioning correctly, it is said to be an $MPPT$.

1.2 Motivation

Clean and renewable energy has greatly increased funding for supporting areas in research and development. Today, energy is necessary for nearly everything. We need a more efficient method of transferral and transformation of DC for different voltages and power levels. By analyzing the power transfer in a buck converter, we will be able to better

understand how and why these converters function so well.

In our modern society, it has become increasingly necessary to shift away from non-renewable resources. A change might occur if energy prices were to increase drastically, but by then it might be too late to switch our focus and essentially rebuild our machines to run off of fuel that is readily available. The effect can be seen today in the car industry as currently it is driven by petroleum. With every increase in petroleum prices, a public outcry is heard and more and more people are replacing their inefficient vehicles with modern hybrid or electric drive vehicles. We can reduce the effect of petroleum pollution by shifting to renewable resources, such as photovoltaics. In addition to this need for renewable resources, there is also a similar need for efficient transformation of power from one form to another.

Since solar panels are quite inefficient to begin with, any method of improving power transfer from these panels is a worthwhile gain in overall efficiency. One method to accomplish this is to operate the panels at their *MPP*. By connecting a solar array to a buck converter, we can control the output voltage of the panels. The parameter to be controlled is the percentage of time a switch is active during each control cycle. In order to compare the performance of different algorithms designed to control the buck converter, a simulation was made to compare the algorithms.

1.3 Technology Overview

In order for the reader to get up to speed, we need to cover the relevant histories of each component. First, the history and important discoveries in photovoltaics is included. These milestones in solar cell history are important because this will further explain the trend of photovoltaic research. Then we will discuss the buck switch mode power converter and its operation. Finally, the chapters' contents will be described.

1.3.1 Solar Cells

The late 1800s were the beginning of man's search for the electrical properties of materials. Eleven years after selenium was discovered to have photoconductivity in 1873, the first solar cell was patented by Edward Weston under patent number US389125 [1]. He was only the first in a long line of scientists who were interested in photoconductivity as well as the photovoltaic effect. Albert Einstein published a paper explaining through quantum physics the photoelectic effect [2]. His paper helped many other scientists to understand the mechanism of photovoltaic action and, therefore, this technology has improved over time. Bell labs was the first to lead industry by developing a silicon P-N junction photocell. These first photocells have an efficiency of six percent [3].

The first solar powered satellite was the TIROS-1 launched in 1960 [4]. Previous satellites used batteries that were charged before heading to space and had no way to be recharged in space. Since technology for batteries was in its early stages of development, the power capacity for these small communications relays was quite low until they had a way to recharge the batteries while in space. Seven years later, in 1967, Soyuz 1 was the first manned spacecraft to have its power replenished by solar panels [5]. From that point onward, nearly all satellites have been solar powered.

In 1980, thin film solar cells were developed by a team at the University of Delaware [6]. Thin film cells can use one of four different absorbing semiconductors: $amorphous - Si$, $CdTe$, $CuInSe_2$, and Cu_2S. Depending on which absorbing material is chosen, the efficiency and cost can be greatly affected. The lower cost of manufacturing and low mass encouraged more research into thin film solar cells. In many of today's integrated applications, thin film solar cells are an important component. Their importance is derived from their flexibility and their thinness. Current bulk-silicon-based photovoltaics have a very

thick profile and cannot be bent or deformed even a small amount without shattering.

Recently, there have been many innovations that have allowed photovoltaics with efficiencies greater than 40% to be created by the University of Delaware [7] . While these are still research cells, it says a lot about the future of solar since they have already improved these efficiencies from 10% to 40% in 50 years, as can be seen in Figure 1.1. The time needed to start a new fabrication line as well as the research needed to further optimize new types of manufacturing is usually around ten years; this assumes that production costs are reasonable and their special structures used to achieve the increased efficiency are reproducible.

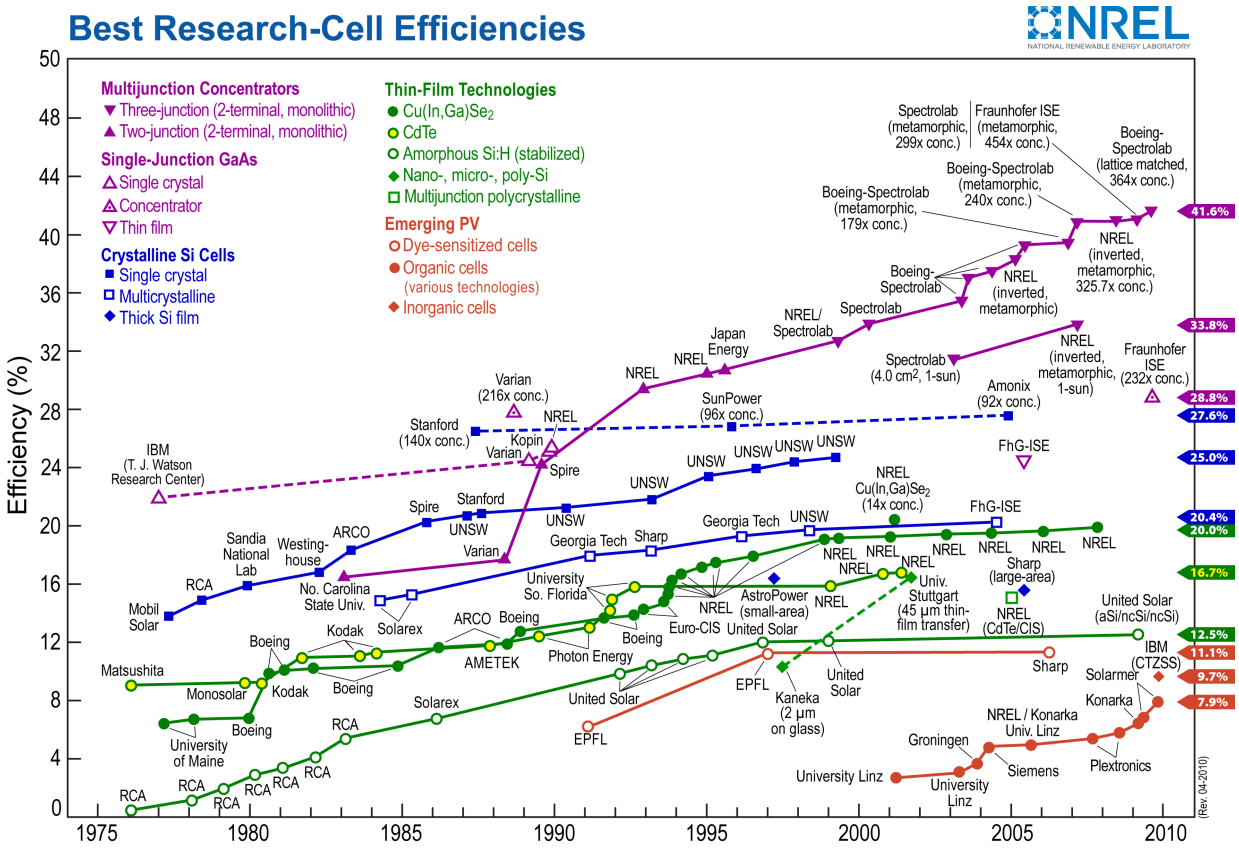

Figure 1.1: Best research solar cells in production by year. Image from [8].

When analyzing a solar cell, efficiency is one of the greatest parameters which is measured. These measurements are done with special lights, solar simulators, which will illuminate

the array with a constant $1000\,W/m^2$ as we see on the surface of Earth. By knowing the total amount of power in the light that is incident on the surface of the cells, the efficiency can be found from

$$\eta = \frac{P_{out}}{P_{in}} \times 100\%, \tag{1.1}$$

where P_{out} is the output power and P_{in} is the input power.

In order to get the correct efficiency measurement of the solar array, we need to normalize based on area. By dividing energy by the area, we obtain the normalized energy output

$$\varepsilon_{norm} = \frac{\varepsilon}{A} \tag{1.2}$$

where ε is solar irradiance energy and A is area of the solar array.

1.3.2 Buck Converter

Output Voltage Ripple

It should be noted that in switch-mode *DC* power supplies, one of the more common metrics to judge the performance of the converter is output voltage ripple. Usually, voltage ripple is on the order of <1% of the total output voltage. Therefore, analysis assuming $v_o(t) = V_o$ is valid. It should be shown that the output ripple is consistent with the discussion of the low-pass filter characteristics of the input [9].

1.4 Thesis Organization

In Chapter 1, background information about solar technology was provided. The current problem with power output from solar panels was described. This information was used to further solve our primary research questions. An overview of the solar cell was discussed

as well as the necessity to convert power between different voltages and currents using a buck switch mode power converter.

In Chapter 2, the literature review of other papers written relating to the following topics is presented: buck converters, solar arrays, or *MPPT*. The differences between this project and referenced papers are discussed. Any improvements made to the circuit or simulation due to the literature review are noted.

In Chapter 3, the functionality of each component in the system is explained. They are modeled in MATLAB to simulate the real-world components. The operation of each circuit component in the system is covered in Section 3.1. The modeling of these components in MATLAB is covered in Section 3.2.

In Chapter 4, test runs on the simulation of the buck converter with *MPPT* control are used to show the efficiency of power conversion. The I-V and P-V curves of the solar panel are also illustrated. How the model is assembled in MATLAB along with any challenges along the way are also described. It was also necessary to test the performance of the model.

Chapter 5 contains a comparison of the three major *MPPT* algorithms and a discussion of how each has its own optimal parameters which can be optimized. The effect of tuning the *MPPT* algorithms through both sample rate and gain of duty cycle change are also shown. We will also compare the output response from each *MPPT* algorithm under each of the three illumination profiles.

Chapter 6 is the conclusion of the thesis. Useful ideas to examine in the future are covered as well as other uses for this type of power converter. Modifications that can be done in order to compensate for changes in design parameters, as well as recommendations to ease future work are also discussed.

THIS PAGE INTENTIONALLY LEFT BLANK

CHAPTER 2:

LITERATURE REVIEW

2.1 Masters Thesis – Hurd

In this thesis, William R. Hurd documented his best effort to use solar cells to increase the endurance of a unmanned air vehicle (*UAV*). In order to optimize the output of his solar panels, he needed to use an *MPPT*. The *MPPT* he chose also contained a battery charging circuit. This simplified his designs to allow him to focus on the actual mounting and positioning of the solar cells. The panels he used were removed from the manufacturer's encapsulation. He then laminated the cells to the top of the air vehicle's wing. A major difference between his project and the one described in this thesis is the voltages of his solar array input and the voltage of his battery system. While his system had a higher battery voltage, the one considered in this thesis has a higher solar array voltage. His design required a boost converter, while the one considered in this thesis requires a buck converter. [10]

2.2 Masters Thesis – Coba

This thesis was very similar in content to William R. Hurd's thesis. Javer V. Coba was attempting to continue the work of Mr. Hurd. Javier Coba was focused on a specific production *UAV*, the Raven RQ-11B. While Mr.Hurd did have the Raven *UAV* in mind, he did not have the chance to test his addition in the field. By their calculations, they nearly doubled the endurance of the unmodified UAV. This improvement did come at a cost as the solar wing they fabricated was too large to fold and store in the original manned portable *UAV* package. Because of this, they concluded that any solar array extension of the Raven

RQ-11B wing system should be done by the company when the wings are manufactured so as to provide a reliable and scaled form factor and still enable a two-man crew to deploy the *UAV* in field. [11]

2.3 Modeling and Simulation of Photovoltaic Module Using MATLAB/Simulink

The steps taken to measure the output of two specific solar array modules, MSX60 and MSX64, were described in this paper. Measurements were taken in order to impliment a model in MATLAB. Datasheet parameters were used as input into the equation describing the current output of the solar panel. They used the model in order to simulate the MPP and graphed the current versus voltage and power versus voltage, showing the higher output panel producing more peak power than the lower rated panel. Their experiements confirmed that the simulation was well matched to the datasheet information. [12]

2.4 Advantage of Boost Versus Buck Topology for Maximum Power Point Tracker in Photovoltaic Systems

Since the buck converter was used to step down the voltage of the solar array, the drawbacks of using buck with a solar array was analyzed. In this paper, they discussed how the use of a buck converter is not optimal for solar arrays. The most important aspect of the experiment is getting as much power out of the panels as possible. While a buck converter is connected to a solar array, it operates the solar array in a state of source discontinuity. This means that while the switch is 'off', the panel is disconnected and no current is flowing from the panel to the converter. This state can be considered pure loss. Without a continuous connection to harness the output of the panel, all energy that would have been collected while the switch is in the 'off' position is lost. The way to circumvent this problem is to add a large input

capacitor, which can store at least the same amount of charge that is generated while the panel is disconnected from the converter.

In general the buck converter has a control advantage. While the boost has a right-half plane zero, the buck does not. This right-half plane zero causes the response of the boost converter to first fluctuate in the opposite direction prior to correcting itself. [13]

2.5 Comparison of *MPPT* Algorithms for $DC-DC$ Converters Based PV Systems

The differences between two popular *MPPT* algorithms, *P&O* and *InC* were described in this paper. In order to get a good metric for comparison, the authors designed both power conversion circuits to be optimal for that specific algorithm. This was done to compare the algorithms on an even footing. The conclusion they draw is that the best controller is *InC*, but if you consider increased cost of implementation of the optimal circuit, then *P&O* gains favor. Due to the lower cost of measurement devices needed for the algorithm, Perturb and Observe is the most cost effective and efficient *MPPT* algorithm. [14]

2.6 High Efficiency Switched Capacitor Buck-Boost Converter for PV Application

A switching capacitor buck-boost hybrid converter for module level distributed-*MPPT* PV applications was introduced and described in this paper. The operation principle of the proposed converter is covered including the detailed operating of a resonant charge pump converter. This converter achieved 92.5% efficiency in the experiment. While not very similar to the application described in this thesis, it is good to have a few sources which discuss other methods of implimentation of power converters. [15]

2.7 A Novel *MPPT* Charge Regulator for a Photovoltaic Stand-alone Telecommunication System

A commercial *MPPT*, SIELTE S4007 with their own converter which uses a two-phase synchronous buck topology was discussed in this paper. They found that there was a significant loss in power when using the SIELTE module to track the *MPP*. Its error from ideal was always greater than 5%. It is interesting to note the way that they implimented the two-phase synchronous buck topology. They used Kyocera 125-G2 panel as the basis for their circuit simulator model. [16]

2.8 Improved Circuit Model of Photovoltaic Array

In this paper, the authors first explain the current circuit model of how a photovoltaic array functions. They improve upon the model by using a next order piecewise linear mathematical model. They were able to accomplish this by measuring the output of a real panel under known insolation and temperature. By using those measurements as data points on a piecewise function to model the photovoltaic array, they showed that this model was able to account for mismatched panels connected together as well as partial shading of sections of the array. [17]

2.9 Comparitive Study of Maximum Power Point Tracking Algorithms

The most common algorithm for *MPPT* is *P&O*, yet it is explained in this paper that it is not the most efficient algorithm. The most common reason for using *P&O* is the simplicity of the circuit. This leads to the negation of need for a complicated processing unit. Their main goal was to evenly compare the algorithms across equivalently optimized hardware as well

as with the algorithms optimized for that hardware. They conclude that the increase in cost of implementation of *InC* greatly outweighs any improvement in efficiency gained. [18]

2.10 Design and Implimentation of Maximum Power Point Tracking Algorithm for a Standalone PV System

Using a model based on Simulink blocks in MATLAB, the authors simulated the action of an *MPPT* system. With a variable irradiance from the solar array, the authors use an *MPPT* algorithm to control a boost converter driving a resistive load. In this paper, the authors compare *P&O* with *InC*. They note that tuning the algorithm using incremental changes is important for both algorithms. *InC* uses far more complicated calculations and, thus, requires more powerful hardware when physically implemented. [19]

THIS PAGE INTENTIONALLY LEFT BLANK

CHAPTER 3:

SYSTEM OVERVIEW

3.1 System Diagram and Description

In this chapter, the use of MATLAB with Simscape, SimPowerSystems and SimElectronics toolboxes to simulate the complete system as seen in Figure 3.1 are described.

Initially, sunlight hits the solar panel array. After being recombined in the active region of the solar cell, the electrons flow into a buck converter. The buck converter then lowers the voltage and increases the current. Control of this converter is provided by an *MPPT* algorithm, which monitors the solar array output and uses the current and voltage measurements from the array to track the highest power output of the array.

One such *MPPT* algorithm will perturb the output setting and then observe by measurement the change in output power. When the power reaches the *MPP*, the algorithm will stop changing the setpoint for the duty cycle (D). One of the parameters to investigate how it effects the overall system is the sampling rate and how often the *MPPT* will change the D of the buck converter. If the sampling rate is too fast, the new D might oscillate around the actual *MPP*, thereby, never extracting the maximum amount of power. On top of that, there might be a transient instability created by not allowing the step response of the output voltage to settle after changing the setpoint of D.

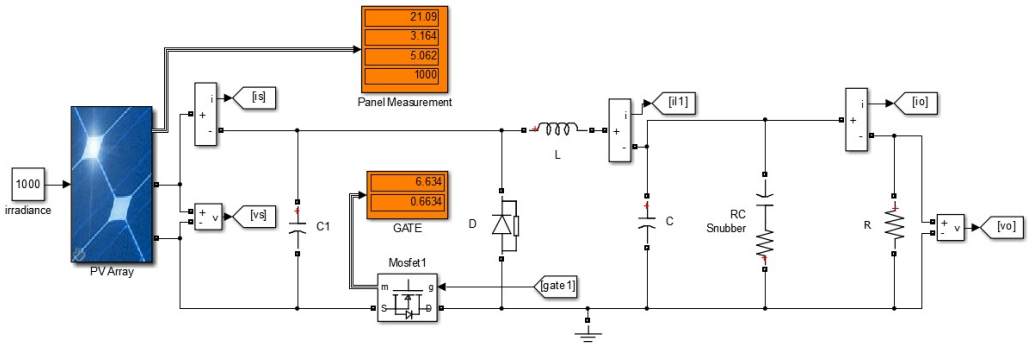

Figure 3.1: The functional portion of the model under test in Simulink, which includes the solar array, buck converter, and resistive load.

The algorithm will use the *MPP* to set the *D* of the pulse width modulation (*PWM*) for the buck converter. Under proper conditions, the greatest amount of power is transferred to the load with minimal losses. The losses of efficiency in the system are due to *MPP* tracking error, buck converter efficiency, and solar cell conversion efficiency. Due to the lack of discrete resistive circuit elements, a buck converter can operate with efficiencies greater than 95% [9]. The total output power of the buck converter delivered to the load should be at least 95% of the input power from the panels. When the panels react to changes in irradiance, there is a disturbance in the setpoint needed to keep the panels at their *MPP*. During the time while the algorithm is tracking the new *MPP*, there is a small amount of inefficiency attributed to tracking error. This error is based on the irradiance, making it a difficult error to account for in the physical world. In simulation it can be quite easy to measure since we can control the illumination of the panel in a controlled manner. The tracking error will be tested in simulation to use as a metric for comparison of the *MPPT* algorithms.

Measurement of the input and output power are the best metric to determine how well the buck converter, MOSFET, gate drive, and *MPPT* algorithm work together. From this

measurement of input and output power, efficiency can be calculated using Equation 1.1.

3.2 Modeling of Components Under Test

In order to simulate the analog components which are in use for this thesis, we need to use mathematical approximations to what the elements actually do. Without this step, it is difficult to compare these circuits. By using these models we are then able to do discrete analysis with the assistance of a computer for calculations. Calculating these by hand is time prohibitive. In MATLAB there are many blocksets already created to ease the use of their software environment. By connecting these mathematical models, we are able to simulate the circuit and extract close to real-world data. Once the correct tuning has been done in simulation, the data can then be use the data to instantiate a real-world device.

3.2.1 Solar Array

For this component, we created a model of the solar array based on

$$I_d = I_{sat}(e^{\frac{qV_d}{kT}} - 1), \tag{3.1}$$

where I_d is the diode current (A), V_d is the voltage across the diode (V), I_{sat} is the diode reverse saturation current (A), q is the electron charge (1.602×10^{-19}C), k is Boltzmann's constant ($1.381 \times 10^{-23} J/K$), T is the junction temperature (K), and e is Napier's Constant (approximately 2.71828).

As stated by Mohan:

> The cell characteristic at a given irradiance and temperature basically consists of two segments: the constant-voltage segment and the constant-current segment. The current is limited as the cell is short-circuited. The maximum power

condition occurs at the knee of the characteristic where the two segments meet. It is desirable to operate at the *MPP*. Ideally, a pure *DC* current should be drawn from the solar array, though the reduction in delivered power is not very large even in the presence of a fair amount of ripple current. To ensure that the array continues operating at the *MPP*, a *P&O* method is used where at regular intervals the amount of current drawn is perturbed and the resulting power output is observed. If an increased current results in a higher power, it is further increased until power output begins to decline. On the other hand, if an increase in current results in less power than before, then the current is increased until the power output stops increasing and begins to go down. [9]

For this simulation, a solar array that could output greater than $100\,W$ of power was selected. The panel is made by Kyocera, KD135GX-LP. The datasheet for this panel can be found in the Appendix. This panel has a open circuit voltage V_{oc} of $22\,V$ with a short circuit current I_{sc} of $8.4\,A$. The voltage at maximum power V_{mp} is $17.7\,V$ while the current at maximum power I_{mp} is $7.6\,A$. By plugging these values into

$$P = I \times V, \tag{3.2}$$

we attain $134.5\,W$ of output power from the solar array under full solar illumination.

In order to model the varying amount of shading and cloud cover, a profile of illumination was devised that will check the *MPPT*'s ability to change setpoints within a reasonable amount of time.

By varying the incident illumination of the solar array as well as the output resistance, we can extract the *Current versus Voltage* and *Power versus Voltage* graphs to find the *MPP* of

the solar array, seen in Figure 3.2. The peak of the *Power versus Voltage* graph is the *MPP*.

The mathematical model of a diode, given in Equation 3.1, was used and integrated with a controlled current source from SimPowerSystems. With this block, the buck converter can modulate the output power. In Figure 3.3, we can see the Simulink diode model used to generate the current in the solar array model shown in Figure 3.4.

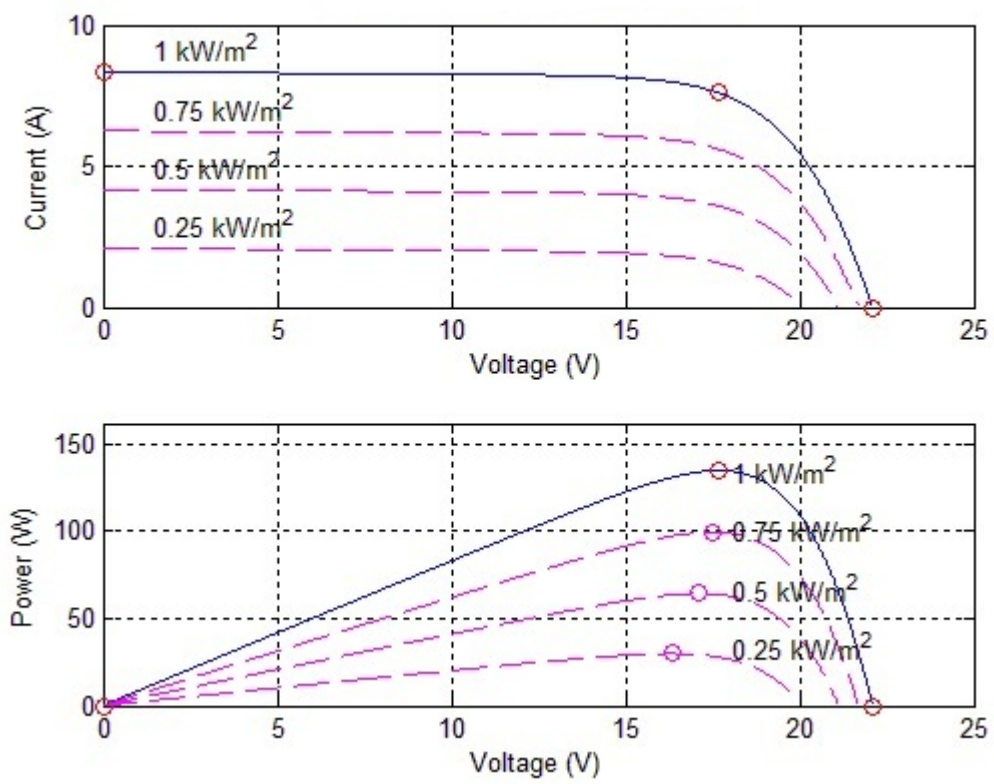

Figure 3.2: The *Current versus Voltage* and *Power versus Voltage* plots from the Kyocera KD135GX-LP panel modeled.

3.2.2 Buck Converter

For the buck converter, we modified the standard topology by moving the MOSFET to the ground leg of the circuit. This was done to reduce the large voltage spikes which might cause damage to the components. The improved circuit is illustrated in Figure 3.5. The

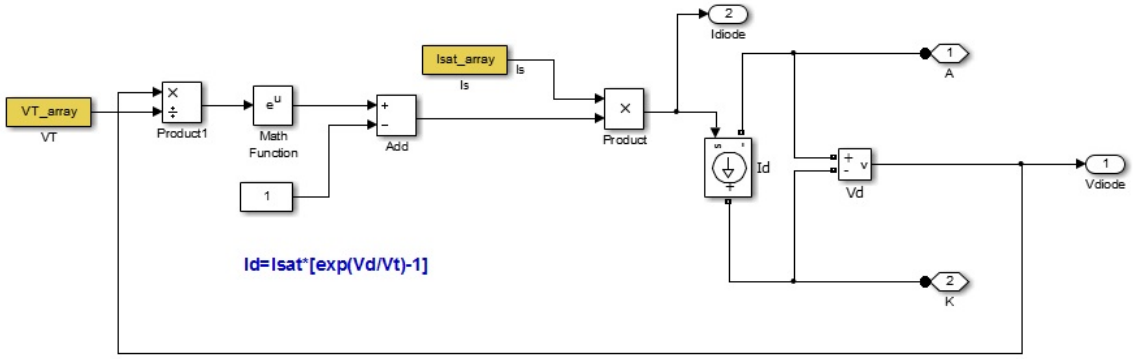

Figure 3.3: The model of a diode which is used within the solar array model.

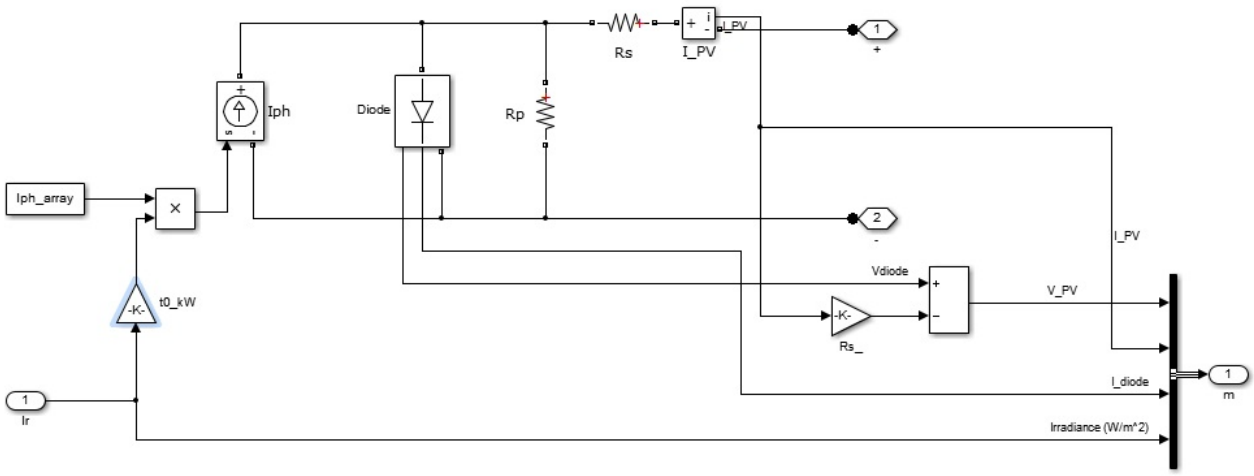

Figure 3.4: The solar array model used to simulate the Kyocera KD135GX-LP panel.

input is coming from the solar array. The output is being modeled as a resistive load for simplicity. The MATLAB circuit model for the buck converter can be seen in Figure 3.6.

The buck converter is a switched mode power supply, meaning it provides digital control through PWM of a switch resulting in a linear response in output voltage. It uses a two switches, a transistor and a diode, and an inductor to continually maintain a voltage on the

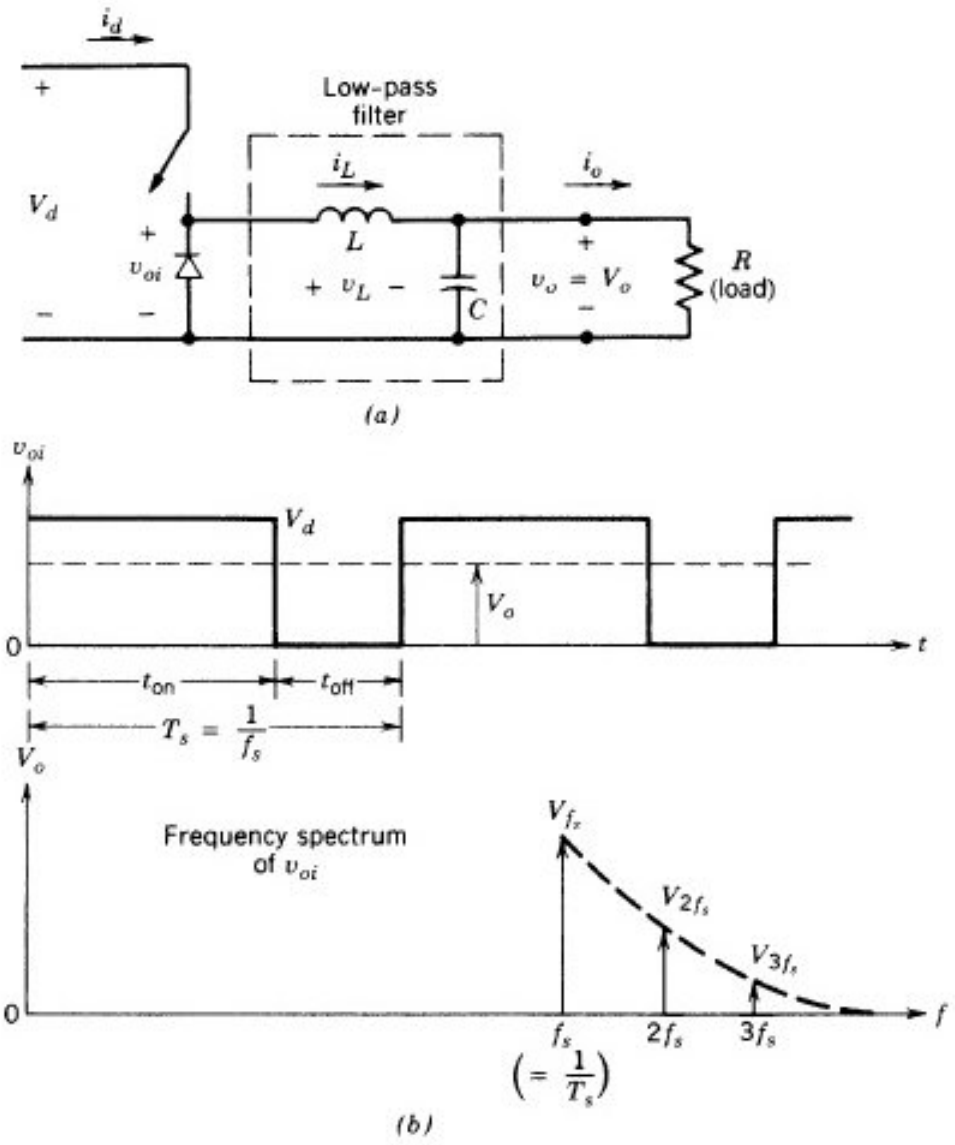

Figure 3.5: Bucking $DC-DC$ converter showing simple circuit diagram (a), output voltage and frequency spectrum of output (b). Image from [9].

output capacitor. Buck converters are commonly used when the input voltage is too high and needs to be lowered to an appropriate level. A step down converter produces a lower average output voltage than the *DC* input voltage V_d. Its main application is in regulated *DC* power supplies and *DC* motor speed control [9].

The v_{oi} waveform in part (b) of Figure 3.5 is shown as a function of switch position. This

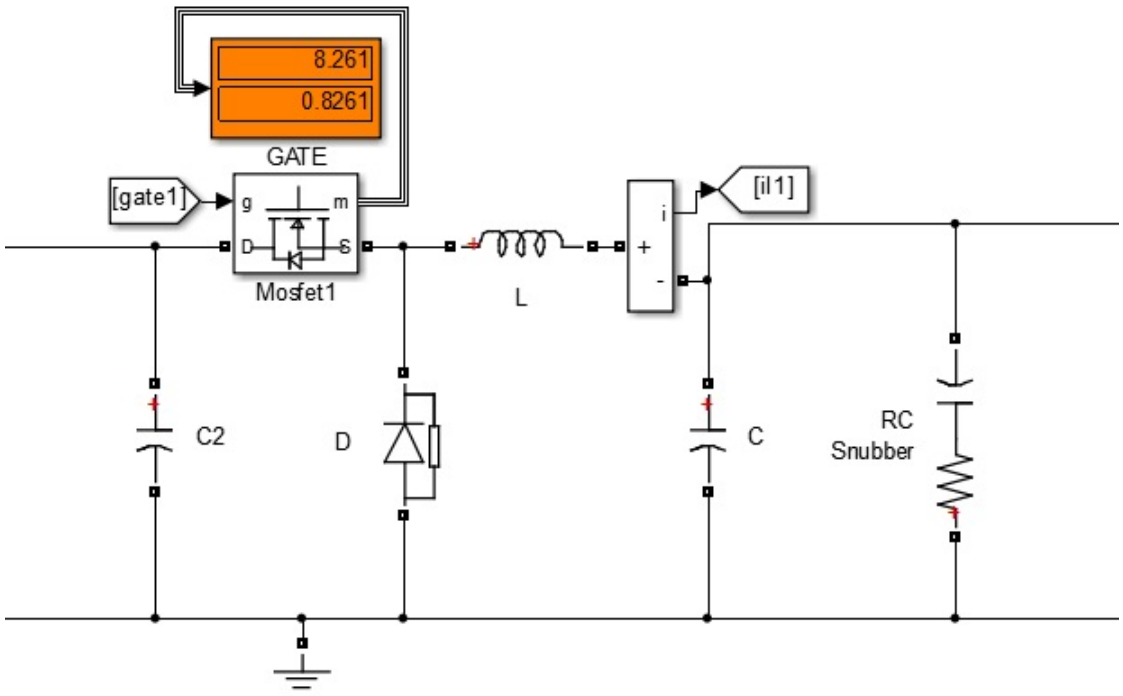

Figure 3.6: Overview of the buck converter model in Simulink.

waveform is what appears at the input to the low-pass filter in part (a) of Figure 3.5. The average output voltage can be calculated in terms of switch's D using

$$V_o = \frac{1}{T_s}\int_0^{T_s} v_o(t)dt = \frac{1}{T_s}\left(\int_0^{t_{on}} V_d dt + \int_{t_{on}}^{T_s} 0dt\right) = \frac{t_{on}}{T_s}V_d = DV_d \tag{3.3}$$

where, V_o is the *DC* output voltage, T_s is the switching period, $v_o(t)$ is the instantaneous output voltage as a function of time, t_{on} is the duration the switch is on per switching period, V_d is the *DC* input voltage, and D is the duty cycle of the converter.

When the active time of the switch t_{on} increases, it increases the *DC* voltage at the output.

The D is related to the 'on' time of the switch divided by the period of switching:

$$D = \frac{t_{on}}{T_s}. \tag{3.4}$$

Any linear change in the duty cycle parameter causes a linear change in the output voltage V_o [9].

As stated by Mohan:

> In actual applications, the forgoing circuit has two drawbacks: (1) In practice the load would be inductive. Even with a resistive load, there would always be certain associated stray inductance. This means that the switch would have to absorb the inductive energy and therefore it may be destroyed. (2) Without the LC filter, the output voltage fluctuates between zero and V_d, which is not acceptable in most applications. [9]

Normally, the combination of an active inductor serially connected to a capacitor would cause arcing across a switch trying to disconnect the source current. To provide an alternate current path while the switch has disconnected the source, a diode is included in the circuit. By employing the use of a low-pass filter, an inductor and capacitor combination as shown in Figure 3.7, the output voltage and current fluctuations delivered to the load are greatly reduced.

The corner frequency f_c of this low-pass filter is calculated from

$$f_c = \frac{1}{2\pi\sqrt{LC}}. \tag{3.5}$$

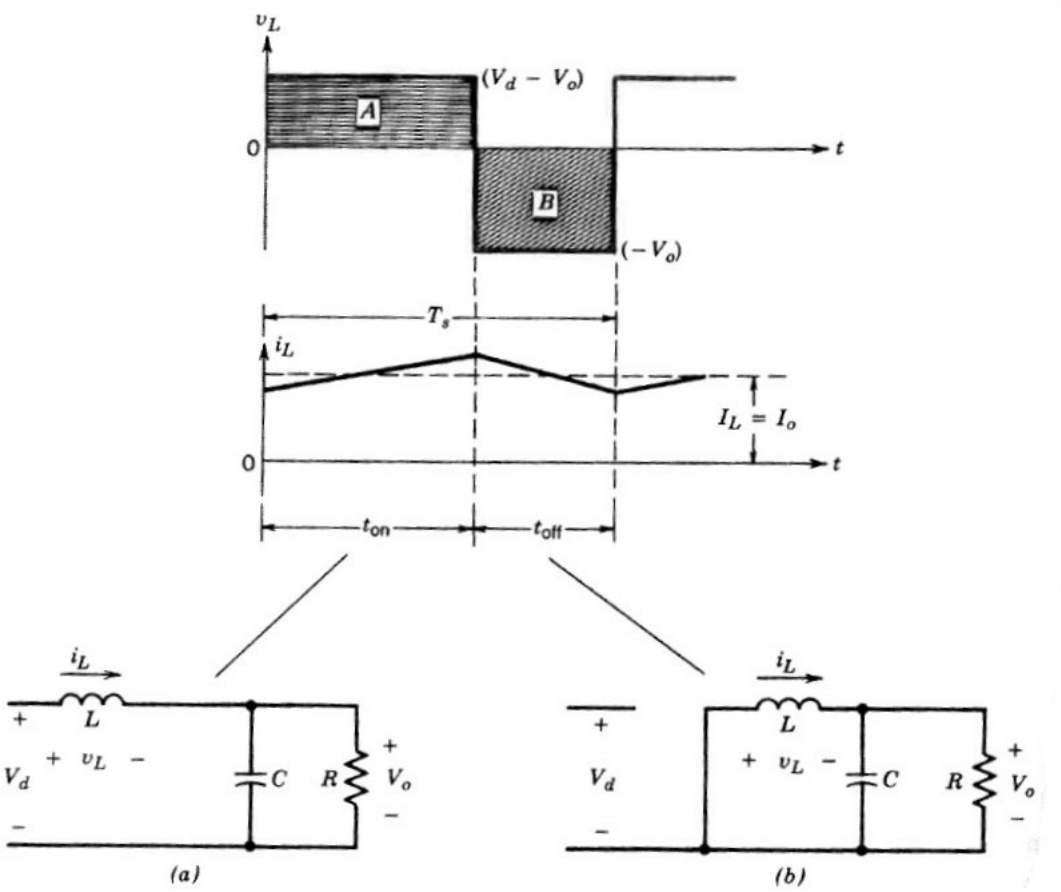

Figure 3.7: Buck converter in continuous conduciton mode with switch on in part (a) and off in part (b). Image from [9]

The filter cut-off frequency is selected to be much lower than the switching frequency of the converter, which reduces the output voltage ripple to a reasonable level [9].

During the interval when the switch is ‘on’, the diode is reverse biased, and the input provides energy to the load as well as the inductor. During the interval when the switch is ‘off’, the inductor current flows through the diode transferring some of its stored energy to the load.

This switching can cause some ripple in the output voltage. Due to the nature of inductors, the current needs to ramp up until the switching event occurs again. During this time, the

small changes in current induces a ripple on the output voltage as seen in Figure 3.8.

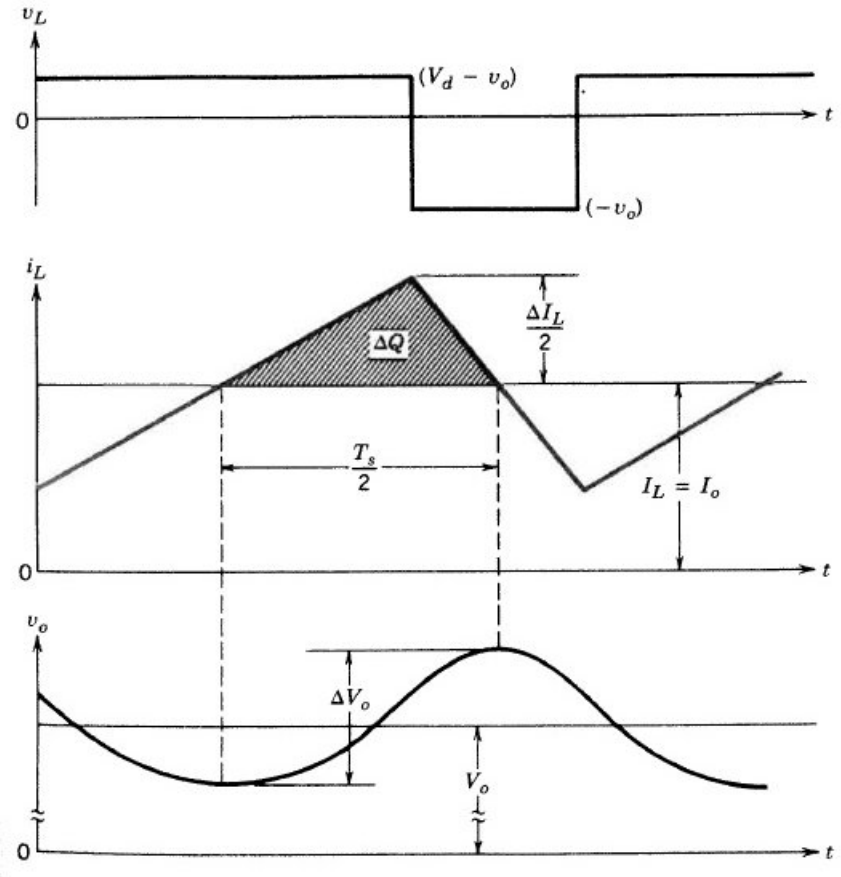

Figure 3.8: Ripple found in output voltage, V_o. Image from [9]

3.2.3 Load

Simulating an active load can be very complex. In order to optimize the buck converter and *MPPT* algorithm during simulation, a resistive load that remains constant through each test was used. The first order model of the output load can be seen in Figure 3.9.

The *MPPT* controller adjusts the D of the buck converter to match the *MPP* of the array, thereby, optimizing output power. By analyzing the output voltage, we can evaluate the effectiveness of the buck converter.

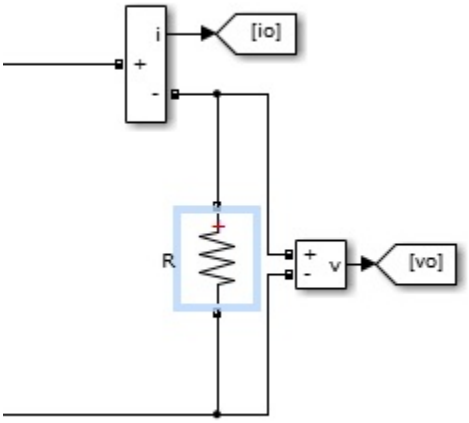

Figure 3.9: Output load resistor with measurement blocks connected.

3.2.4 MOSFET

The MATLAB model as seen in Figure 3.10 for a MOSFET is quite extensive. The adjustable parameters are the FET resistance R_{on}, the internal diode inductance L_{on}, the internal diode resistance R_d, the internal diode forward voltage V_f, the snubber resistance R_s, and the snubber capacitance C_s.

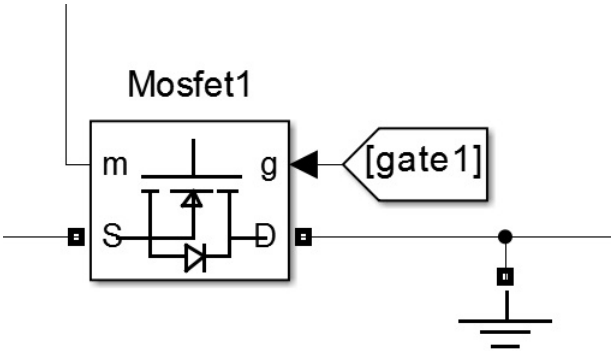

Figure 3.10: MOSFET block from MATLAB SimPowerSystems

3.2.5 Pulse Width Modulation Generation

For simulations in MATLAB, a gate drive circuit model is not necessary since the gating function assumes an ideal switch. The model for a MOSFET was found in the MATLAB blockset SimPowerSystems as seen in Figure 3.10.

The MOSFET gate control for the model can be seen in Figure 3.11. The percentage of time the switch is 'on' for a set switching speed is D. We can use the comparison of D with a triangle wave that ranges from zero to one. When the value of the triangle waveform is higher than D, the MOSFET is 'off'. Similarly, when the value of the triangle waveform is lower than D, the MOSFET is 'on'.

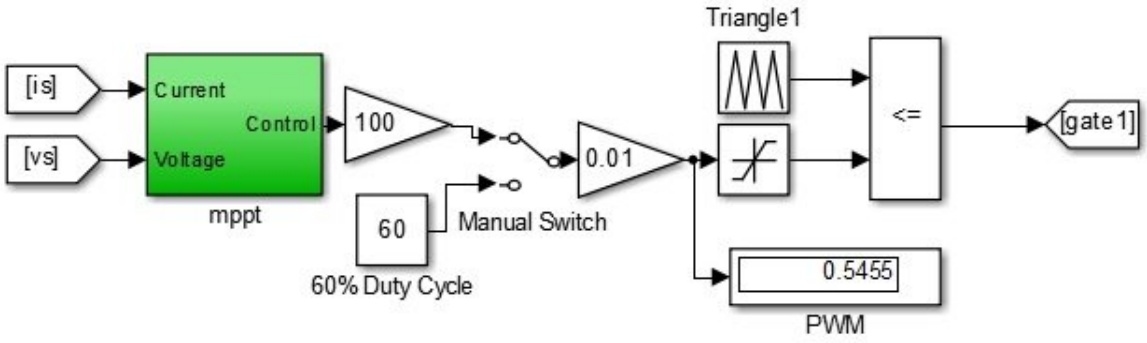

Figure 3.11: PWM signal with triangle wave and duty cycle example

For the MATLAB model, only a binary signal is needed to control the gate. Using this simplified idea of the gate, we can compare the duty cycle with a triangle waveform set to repeat every $40\,\mu s$ with the peak of the triangle at $20\,\mu s$. This gives a control frequency f_s of $25\,kHz$ when calculated with

$$f_s = \frac{1}{T_s}. \tag{3.6}$$

When the value of D is less than than the triangle waveform the output goes to 'one'.

3.2.6 *MPPT* Algorithms

There are many ways to track an *MPP*. In this section, two of the most popular *MPPT* algorithms *P&O* and *InC* are compared.

The perturb and observe (*P&O*) algorithm for finding the *MPP* is widely used in commercial applications. This method uses current and voltage sensors to measure the output of a solar array. The *P&O* algorithm can be the cheapest to implement. Generally, *P&O* is also the simplest to implement due to its reliance on passive element circuits to measure the current and voltage. These measurements are the only outside data sources the *MPPT* algorithm needs to determine whether to increase or decrease the duty cycle. By comparing the input power to the previously measured input power, we can determine whether to lower or raise the duty cycle to continue tracking the *MPP*.

By changing the duty cycle after a set amount of time, the *P&O* algorithm checks the previously measured input power. If the newly measured input power is greater than the previously measured input power and the new input voltage is greater than the old input voltage, it decreases D to move closer to the peak power. If the input voltage was less than previously measured and it had greater input power, the algorithm increases D.

If the new power measured is less than previously measured and the new voltage is greater than the old voltage, D decreases to converge to an *MPP*. Finally, if the power and voltage are less than previously measured, the algorithm decreases D. This algorithmic flow chart can be seen in Figure 3.12.

There are a few optimizable parameters within this algorithm. First, the f_s can affect the size requirement for the inductor and capacitor. If f_s increases, then the sizes of the inductor and capacitor decreases. Secondly, the amount of change in duty cycle can be modulated to quickly converge from large tracking errors. This ΔD is essentially the gain of the con-

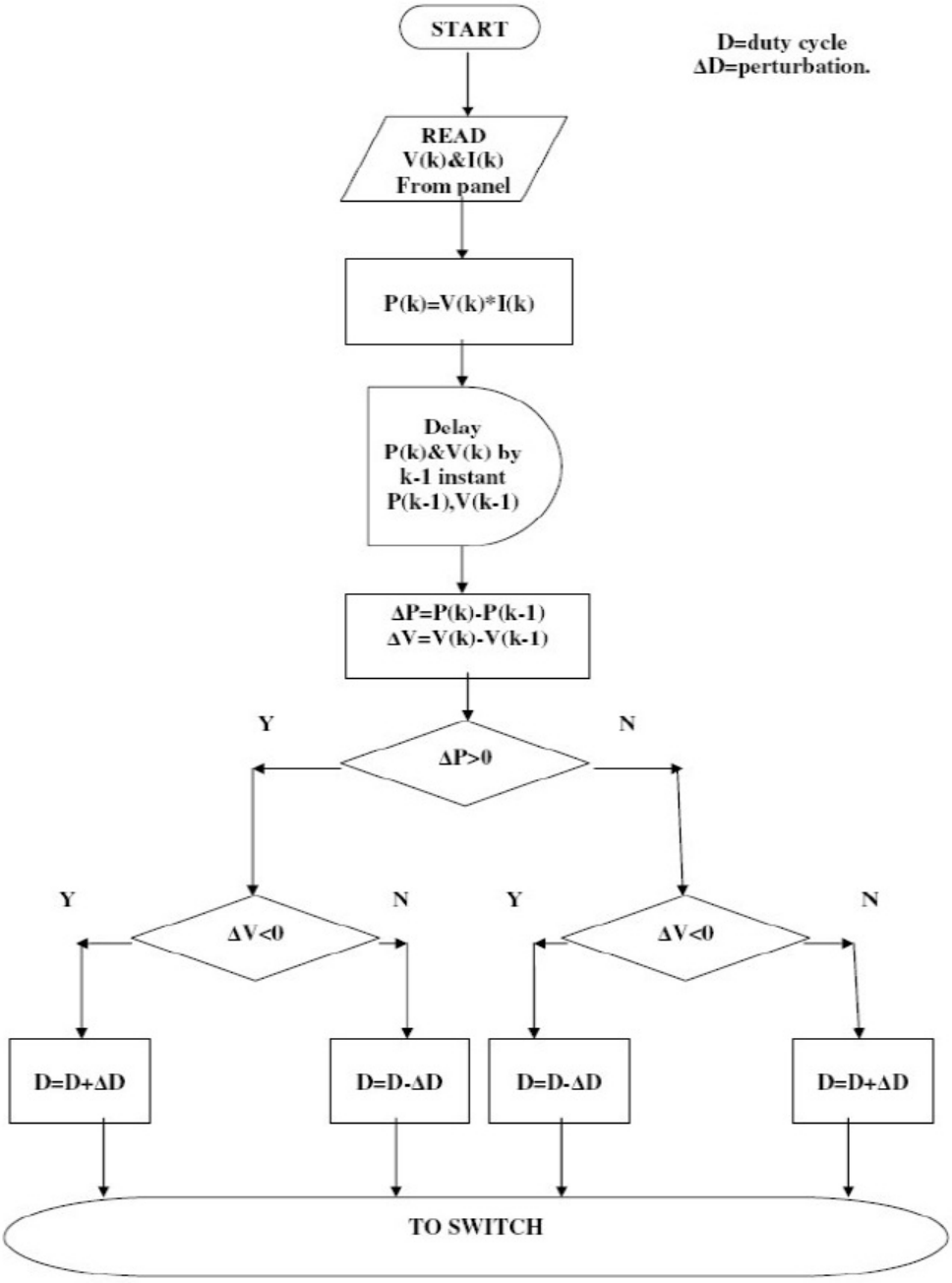

Figure 3.12: Flow chart of Perturb and Observe Algorithm. Image from [20].

troller. If the ΔD is too high it can overshoot and oscillate indefinitely around the optimal point, yet never reach it.

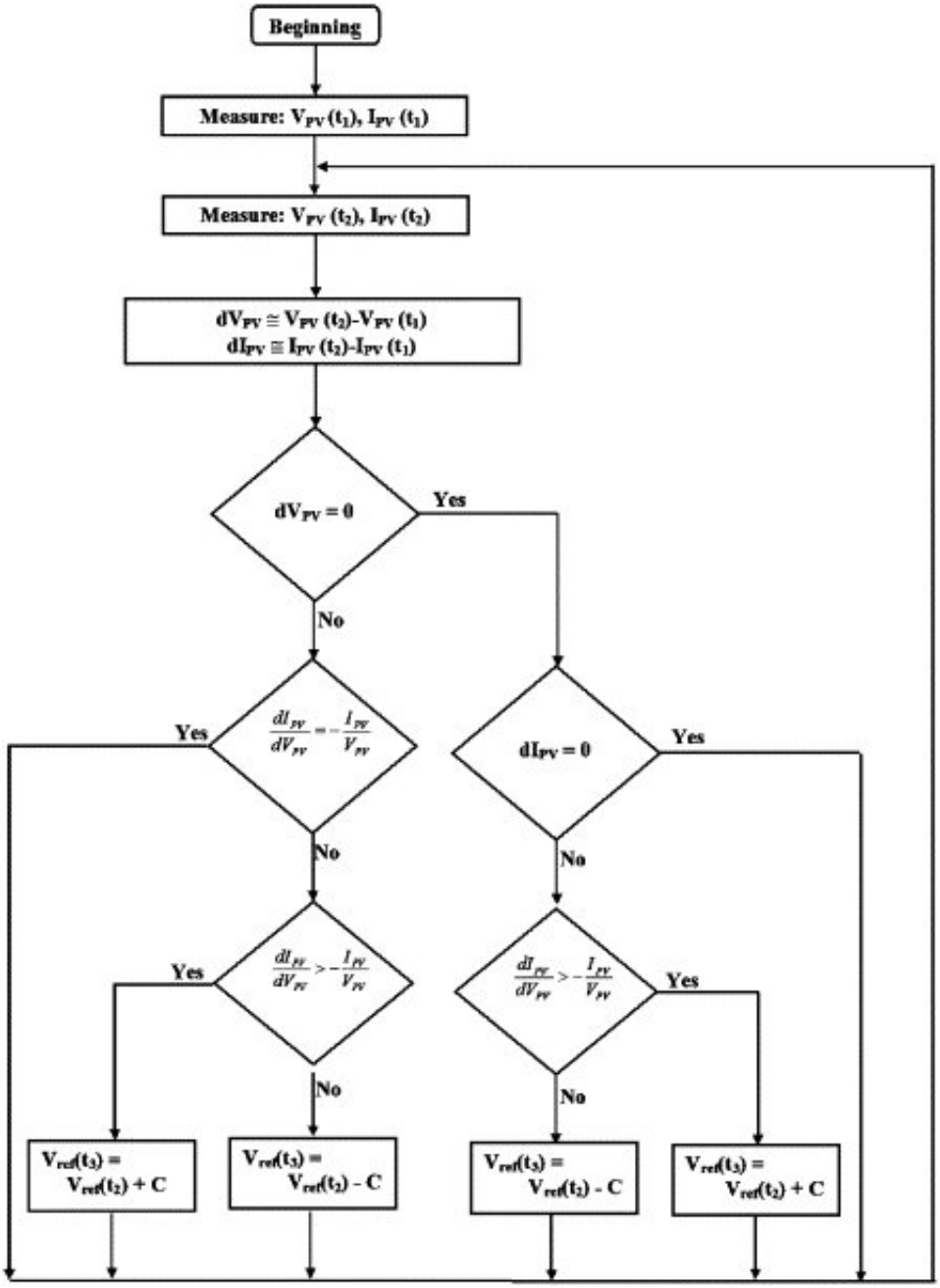

Figure 3.13: Flow chart of the *InC* Algorithm. Image from [21].

The incremental conductance algorithm (*InC*) is another method of *MPP* tracking. This algorithm uses incremental measurements on the change in conductance of the photovoltaic array. By comparing these calculated incremental measurements, we can calculate whether

there was an increase or decrease in power since it was last measured. The incremental conductance is defined as $(\Delta I_{PV}/\Delta V_{PV})$. By comparing this measurement to the actual conductance of the photovoltaic array, one can determine which side of the *MPP* the current operating point is located. "*InC* can track rapidly increasing and decreasing irradiance conditions with higher accuracy than *P&O*. One disadvantage of this is the increased complexity when compared with *P&O* [20]."

The algorithm used can be seen as a flow chart in Figure 3.13. This algorithm has fewer branches for each node and is less complicated than the *P&O* algorithm's flowchart; however, the simplicity of the algorithm flowchart does not account for the increased complexity of binary calculations required for this algorithm.

Since calculation of both the *InC* and conductance requires the use of division, a large amount of processing power is necessary in order to acquire the result before the next sample time. If the calculation to find the *InC* carries over into the next sample time, the controller will be controlling the buck converter further in the past the longer the system runs. If we have each calculation occur as fast as possible by using more power hungry processors with the hardware to perform division, we will be able to appropriately use the calculations for this algorithm and, thereby, optimize the output power.

THIS PAGE INTENTIONALLY LEFT BLANK

CHAPTER 4:

COMPONENT DESIGN

4.1 Requirements and Description

For this simulation, the requirements for the proper operation of the buck converter and solar array at the *MPP* are given by a maximum converter input power of $135\,W$, a converter input voltage range of $15\,V - 25\,V$, an output power of $128\,W$, and a conversion efficiency $> 95\%$.

4.2 Simulation Data

By simulating all the designs of the circuit in MATLAB, proof of operation for the buck converter acting to track the *MPP* are produced. Without the ability to simulate the circuit, the amount of time required to tune the circuit as well as select the proper components to handle the power required would be increased. The procurement procedure for acquiring the power components would also incur a great time loss.

4.3 Calculation of Component Values

In order to guarantee continuous current mode (*CCM*) for the buck converter, there are a few requirements that need to be met in order for the circuit to function as required.

4.3.1 Input Capacitor Sizing

In order to store charge while the switch is in the 'off' position, a capacitor is placed at the input to the buck converter. The capacitor stores charge when the buck switch is in the 'off'

state, alleviating source current discontinuity. The value calculated using

$$C_{in(MIN)} = I_o \times \frac{D(1-D)}{V_{pp(MAX)} \times f_s}, \tag{4.1}$$

where $C_{in(MIN)}$ is the minimum capacitor size (F), I_o is the solar array output current (A), $V_{pp(MAX)}$ is the maximum voltage from the solar array (V), and f_s is the switching frequency (Hz), is $3\mu F$ with a D of 0.5.

4.3.2 Switching Frequency

The switching frequency for the MOSFET in the buck converter was computed by inserting T_s used in simulation, $4 \times 10^{-5}\,s$, into Equation 3.6. we obtain a switching frequency of $25\,kHz$. In order to minimize output ripple, it is essential to have the corner frequency of the low-pass filter at the output $f_c \ll f_s$.

4.3.3 Low-Pass Filter Values

As a subset of the buck converter, there is an *LC* low-pass filter present on the output. By first solving for L using

$$I_{LB,max} = \frac{T_s V_d}{8L}, \tag{4.2}$$

with V_d set to $15\,V$, T_s set to $40\,\mu s$, and $I_{LB,max}$ set to $4.1\,A$, half of the panels' I_{sc}, we get $27\,\mu H$ for the inductor. While this value is fine in simulation, there might be a slight difficulty finding this specific value in a real-world component.

From this point we need to size the capacitor to have the filter corner frequency f_c be much less than f_s. Two orders of magnitude in frequency is usually sufficient to remove f_s from the output. Since f_s is $25\,kHz$, we would like our filter to have a f_c of $2000\,Hz$. This will allow almost pure *DC* to pass to the output, reducing the ripple in current and voltage. By

inputting our previously found value for L into

$$f_c = \frac{1}{2\pi\sqrt{LC}}, \tag{4.3}$$

we can solve for C. The calculated value for C in the output filter portion of the buck converter is $234\,\mu F$.

4.3.4 Duty Cycle

The duty cycle D is modulated in our simulation by the controlling algorithm. By varying D to control the solar arrays' operating point, we see that the output voltage is the input voltage times D using

$$D = \frac{V_o}{V_d} = \frac{t_{on}}{T_s}. \tag{4.4}$$

Since the main purpose is to extract as much power from the solar array as possible, it is important to note that the output voltage will be unregulated unless energy storage is placed at the output of the buck or the resistance is sized such that the buck does not become saturated ($D = 1$). The additional work required will be discussed in Chapter 6.

4.3.5 Desired Maximum Output Voltage Ripple

To calculate the maximum voltage ripple of the circuit, we can input the parameters found in the previous sections of this chapter into

$$\Delta V_o = \frac{T_s}{8C}\frac{V_o}{L}(1-D)T_s. \tag{4.5}$$

An output ripple voltage of $< 1\%$ is desired in most cases.

THIS PAGE INTENTIONALLY LEFT BLANK

CHAPTER 5:

RESULTS

5.1 Validation of *MPPT* operation

5.1.1 Irradiance Inputs

In order to evaluate the performance of each algorithm with a control, three profiles of irradiance were used to simulate irradiance on the solar array. The first run was a constant irradiance at $1000\,W/m^2$. The next run used a step from $600\,W/m^2$ to $1000\,W/m^2$ as seen in Figure 5.1. The final input to test the systems algorithmic response was a variable level of irradiance as seen in Figure 5.2. This final test was to see how well each algorithm handled rapidly changing irradiance.

5.2 Tuning of Duty Cycle Increment.

5.2.1 *P&O*

It is quite easy to tune ΔD using *P&O*. Since there is a much longer time between perturbations, approximately 1000 cycles of the simulation, the output power has more time to settle before the adjustments are made to the set point of D. This is also aided by the two stage gain structure which depends on the error in power. When the difference in power is large, then the ΔD is also large to drive the operating point closer to the *MPP*. Similarly, when there is a small difference in power, then the ΔD is smaller and overshoots less and responds more quickly to small changes in irradiance or temperature.

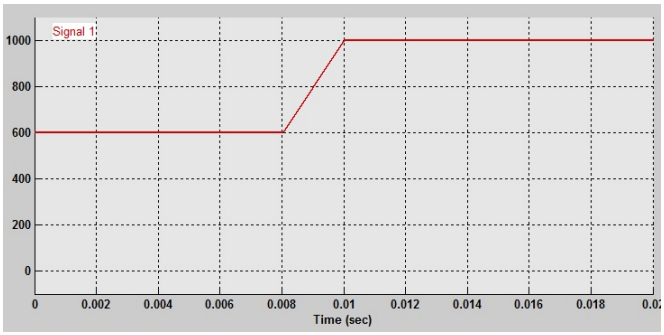

Figure 5.1: The step function used as input to the solar array.

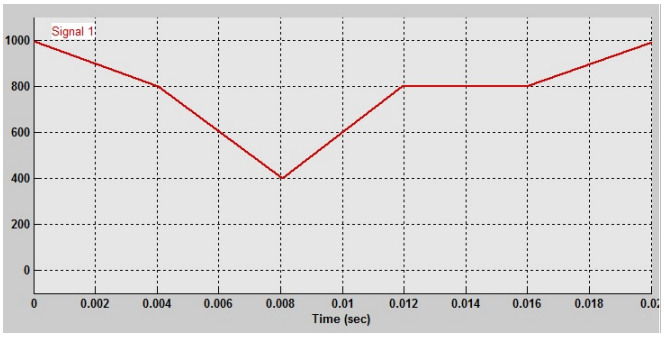

Figure 5.2: Varying levels of irradiance used as input to the solar array in order to mimic passing clouds.

5.2.2 *InC*

While configuring the entire system, the amount of change in D is much smaller than that used in the *P&O* algorithm. Since *InC* uses samples in time much closer together than the *P&O* algorithm, the ΔD needs to be smaller to avoid overshooting the target while measuring previous changes to the set point. Almost all changes in D will cause a normal step response in the output power. By changing the set point of D so frequently, this algorithm does have the aspect of being able to compensate for quick changes in shading or irradiance.

Even after reducing the ΔD to 0.0001, the algorithm still oscillated around the set point desired. This oscillation can be attributed to the control loop speed being too fast as well as the resolution of ΔD being too large. The mathematics required in the algorithm has

Table 5.1: Average overall converter efficiency for the whole simulation time organized by run type.

Run	Overall Efficiency
1 - P&O - Constant	93.42%
2 - P&O - Variable	93.21%
3 - P&O - Step	93.42%
4 - Constant D - Constant	93.29%
5 - Constant D - Step	92.80%
6 - Constant D - Variable	92.64%
7 - InC - Step	93.68%
8 - InC - Variable	93.69%
9 - InC - Constant	93.86%

two checks to see if the change is equal to zero. This can lead to some problems since the change between each reading of voltage and current from the output of the solar array can sometimes contain noise from either a change in set point of D or from either temperature or irradiance change. Further work is required to account for this phenomenon.

5.3 Simulation Results

5.3.1 Power Efficiency

In order to calculate the power efficiency (η) we need to know the maximum power under the given circumstances that the solar array will produce. By integrating both the output power measured and the maximum power, we can calculate the $MPPT$ efficiency (η_{MPPT}) using

$$\eta_{MPPT} = \frac{\int_0^{T_s} p_{out}(t)dt}{\int_0^{T_s} p_{Max}(t)dt}. \tag{5.1}$$

The results can be seen in Table 5.1.

Since this is a simulation, there is a great amount of determinism created by running the same data with different controls. Essentially, the true $MPPT$ can be extracted from the solar array after running the algorithm in order to compute the error in the MPP.

Table 5.2: Percentage of output voltage as ripple organized by run type.

Run	Output Voltage Ripple %
1 - P&O - Constant	0.30%
2 - P&O - Variable	0.42%
3 - P&O - Step	0.15%
4 - Constant D - Constant	0.30%
5 - Constant D - Step	0.30%
6 - Constant D - Variable	0.25%
7 - InC - Step	0.31%
8 - InC - Variable	0.23%
9 - InC - Constant	0.25%

5.3.2 Output Voltage Ripple

The output voltage ripple was calculated from the output voltage versus time plots from each run. The key point to realize is that all the algorithms were being controlled by a tuned buck converter, and therefore, the output voltage ripple while in steady state was well within the specification of $\Delta V_o/V_o < 1\%$ as seen in Table 5.2.

5.4 Comparison of Control Algorithms

By comparing the output waveforms from each run,we obtain a greater understanding of how these algorithms respond to different solar array irradiance changes.

5.4.1 Run 1: Perturb and Observe with Constant Irradiance.

This is the first run of the MATLAB model. This run used an input of constant irradiance to the solar array. The response curve which shows the output voltage has a measurable amount of ripple as seen in Figure 5.4. The current response has a small initial overshoot; then the $MPPT$ controlled the PWM of the gate in order to bring it closer to the MPP, which can be seen in Figure 5.5. The output power remains almost constant from $0.003\,s$ onward as illustrated in Figure 5.6. The converter reaches a steady efficiency of 93.42% and also remains almost completely flat for the rest of the simulation seen in Figure 5.3.

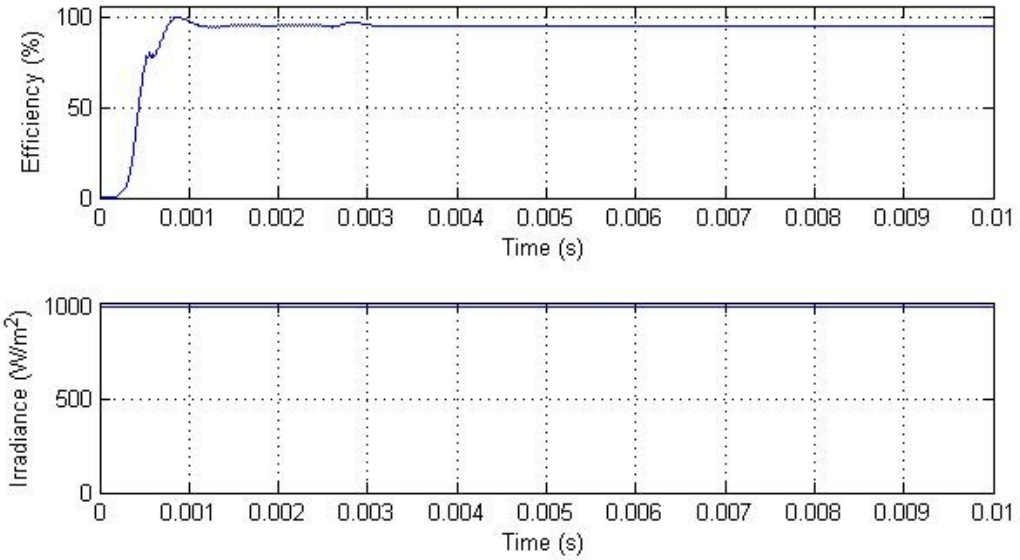

Figure 5.3: *P&O* Run 1. Converter efficiency (top) and irradiance (bottom) versus time.

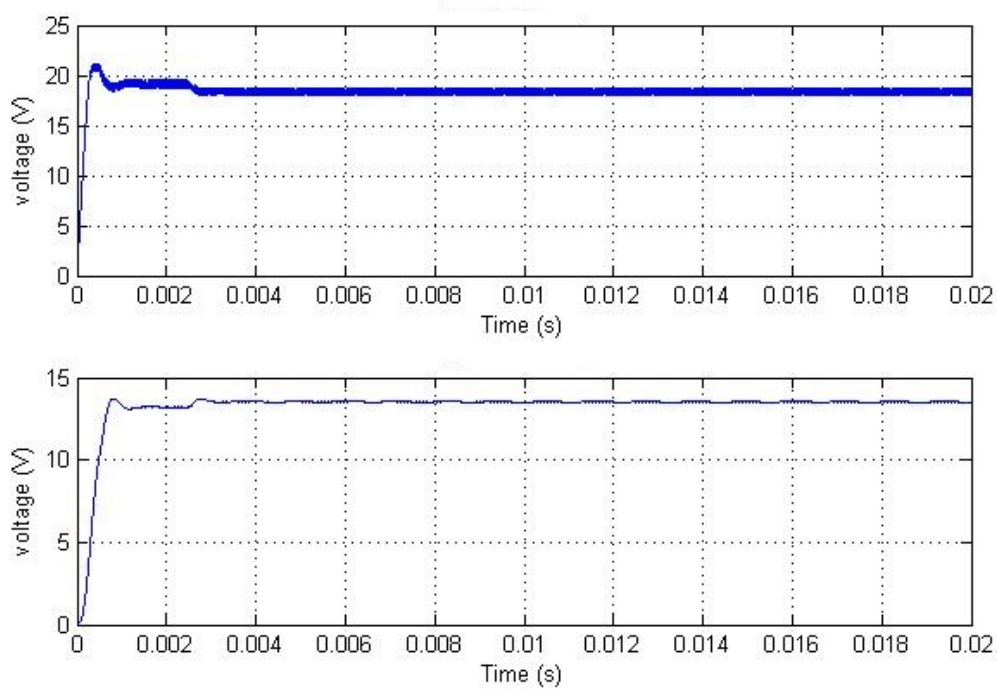

Figure 5.4: *P&O* Run 1. Source voltage (top) and output voltage (bottom) versus time.

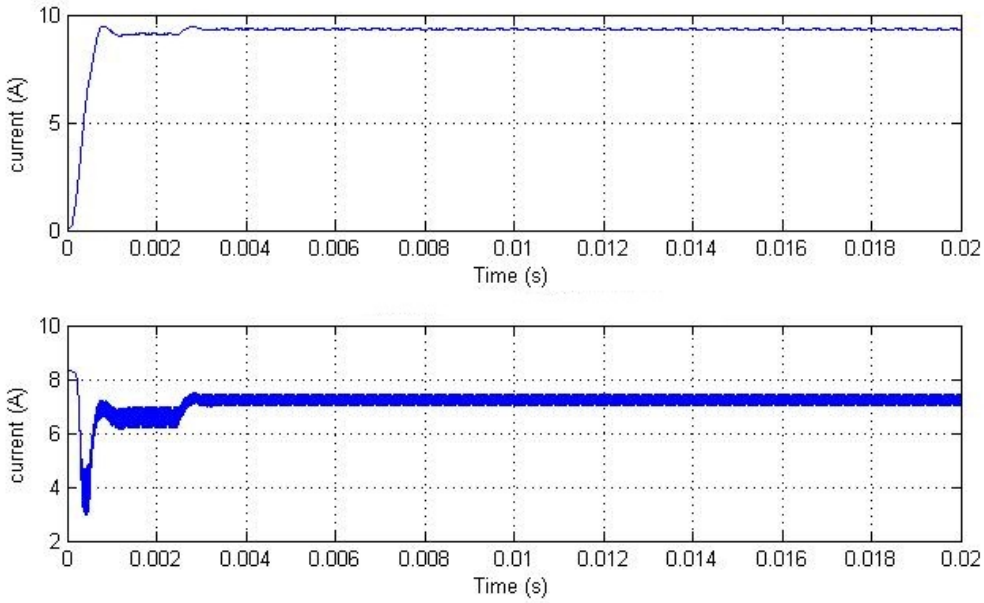

Figure 5.5: *P&O* Run 1. Source current (top) and output inductor current (bottom) versus time.

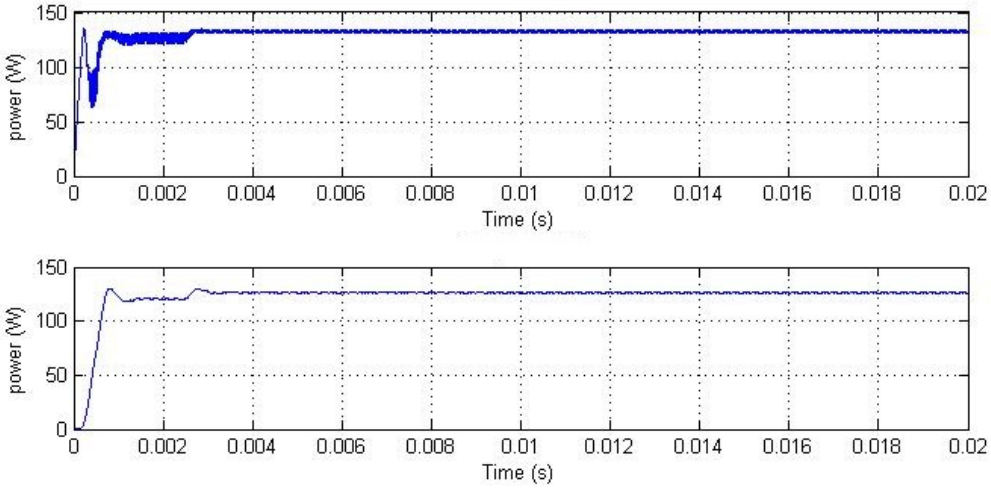

Figure 5.6: *P&O* Run 1. Source power (top) and output power (bottom) versus time.

5.4.2 Run 2: Perturb and Observe with Variable Irradiance.

This is the second run of the MATLAB model. This run used an input of variable irradiance to the solar array. The source and output voltage both track the input irradiance changes as seen in Figure 5.8. The current response has a small initial overshoot at each change in irradiance. The source current tended to oscillate quite a bit when this controller was in operation, which can be seen in Figure 5.5. The output power remains quite close in magnitude compared to the input power, as illustrated in Figure 5.6. The converter efficiency shot above 100% because the input power and output power were averaged over 0.0001 s; therefore, there was a small lag in the input power. Overall, the efficiency did not drop below 80% even with the very abrupt changes in irradiance, seen in Figure 5.3.

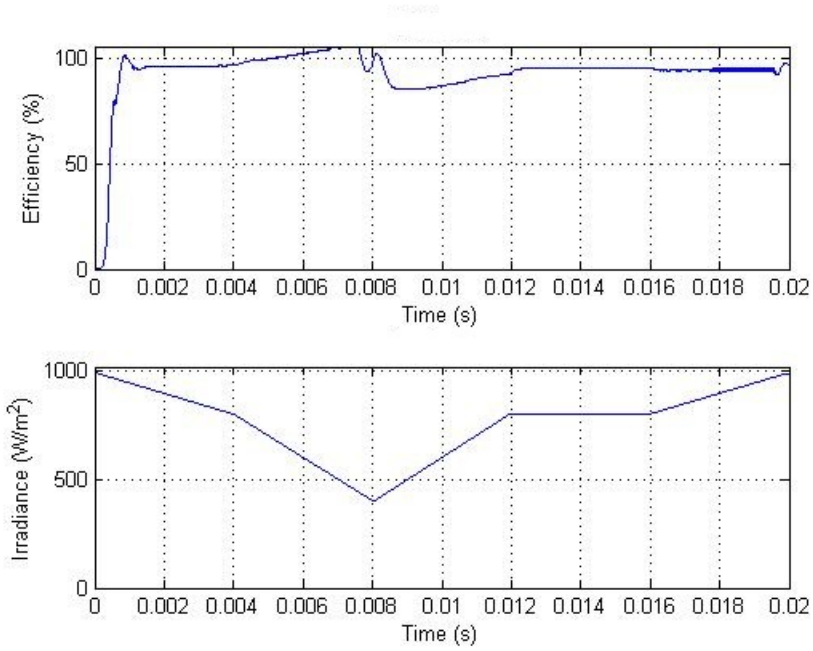

Figure 5.7: Perturb and Observe Algorithm Run 2. Converter efficiency (top) and irradiance (bottom) versus time.

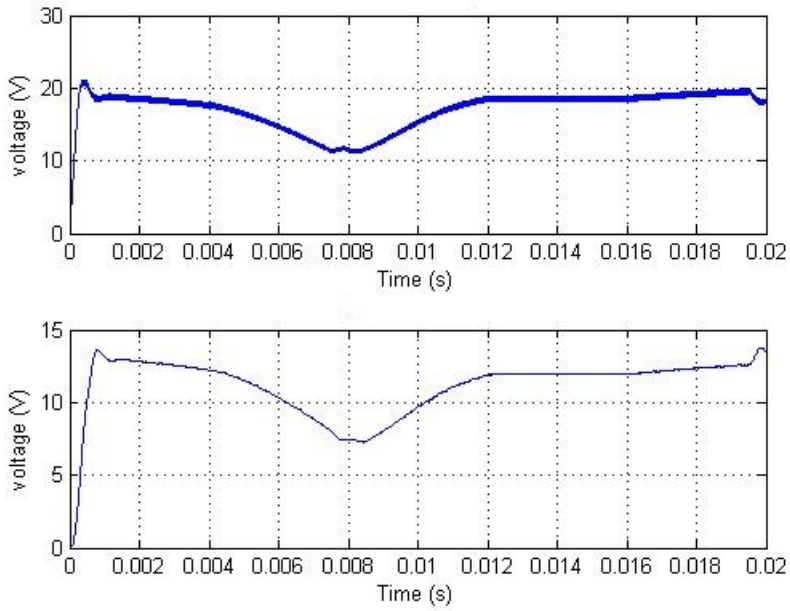

Figure 5.8: Perturb and Observe Algorithm Run 2. Source voltage (top) and output voltage (bottom) versus time.

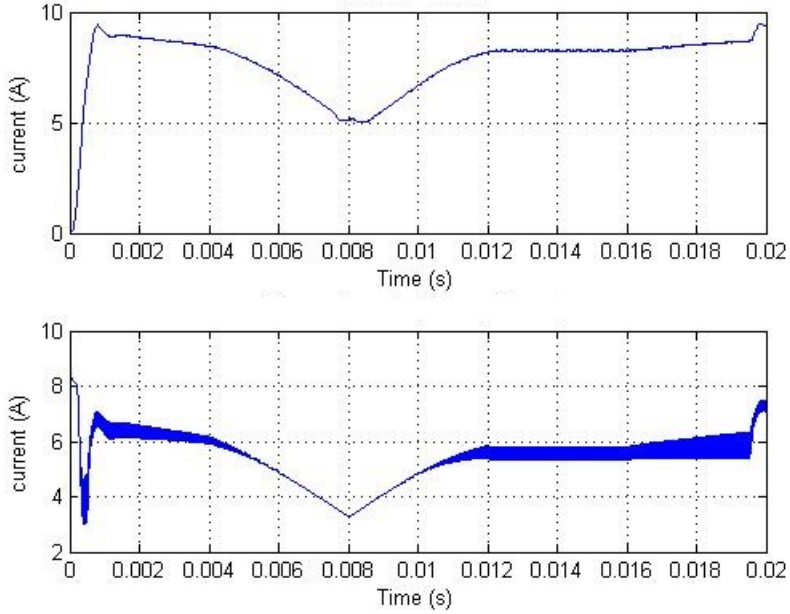

Figure 5.9: Perturb and Observe Algorithm Run 2. Source current (top) and output inductor current (bottom) versus time.

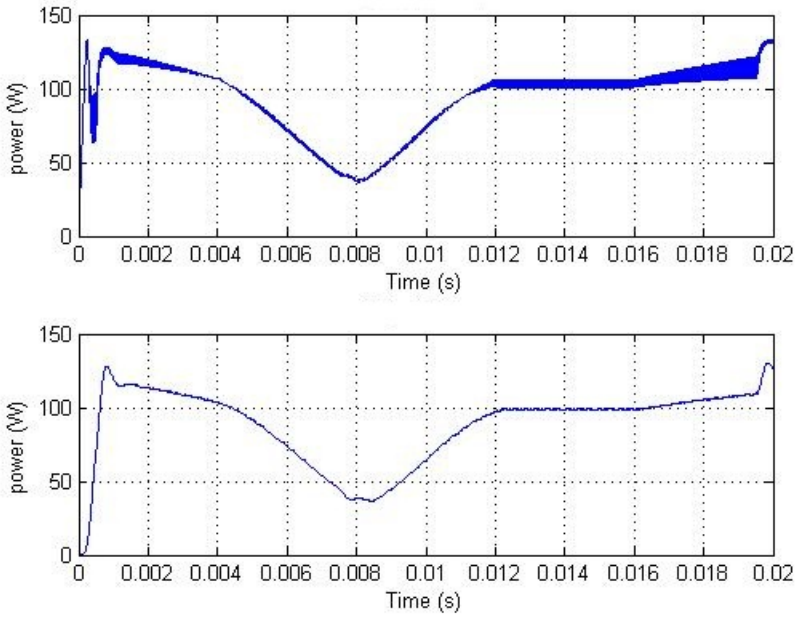

Figure 5.10: Perturb and Observe Algorithm Run 2. Source power (top) and output power (bottom) versus time.

5.4.3 Run 3: Perturb and Observe with Step in Irradiance.

This is the third run of the MATLAB model. This run has a step in irradiance as input to the solar array. The algorithm seems to have corrected in the wrong direction as seen in Figure 5.12. The increase in irradiance was supposed to correspond to an increase in power output. This transient is most likely due to input noise. The source current tended to oscillate only while the irradiance was low, which can be seen in Figure 5.13. The output power eventually did recover after around $0.002\,s$ which is the sample rate of the algorithm, as illustrated in Figure 5.14. The output power during this incorrect swing was around $10\,W$. The converter efficiency had a very unstable section that corresponded to tracking the incorrect direction of the MPP. The efficiency momentarily dropped to 25%, which is illustrated in Figure 5.11.

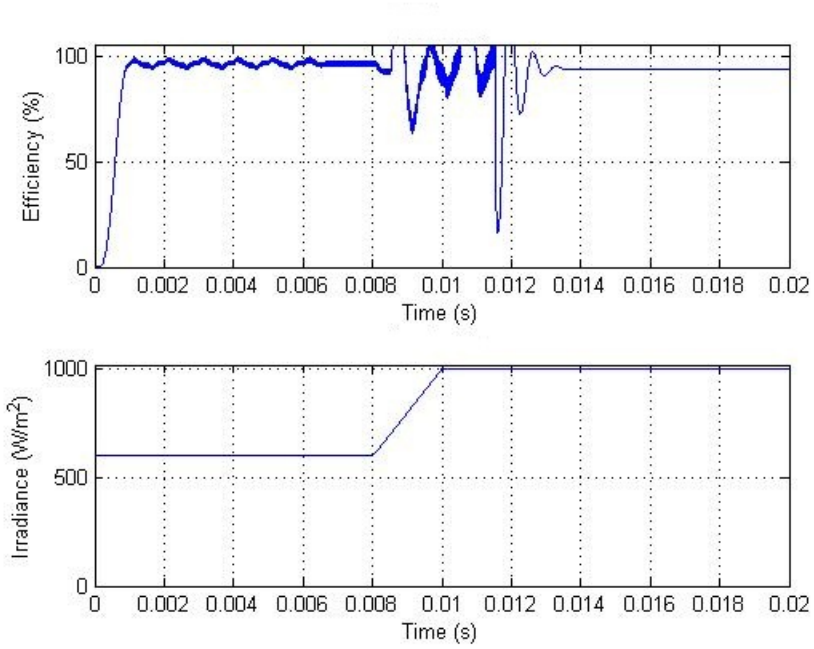

Figure 5.11: Perturb and Observe Algorithm Run 3. Converter efficiency (top) and irradiance (bottom) versus time.

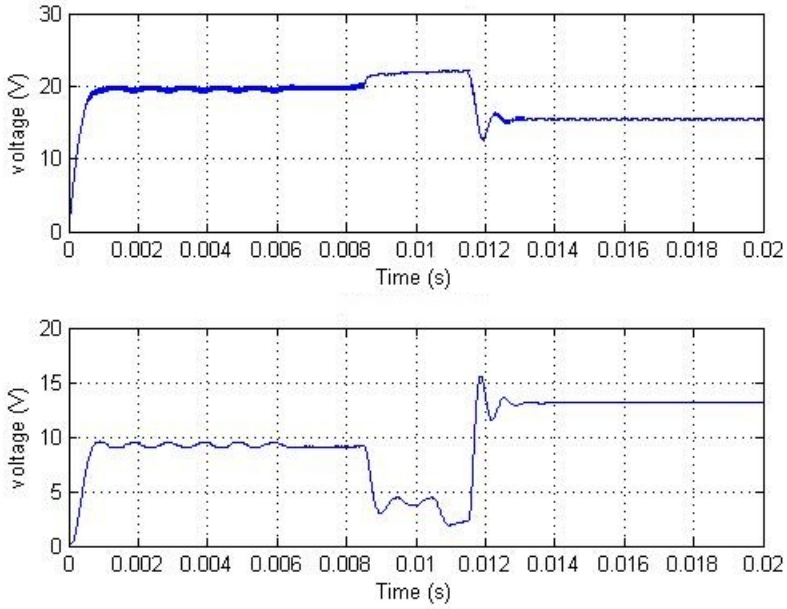

Figure 5.12: Perturb and Observe Algorithm Run 3. Source voltage (top) and output voltage (bottom) versus time.

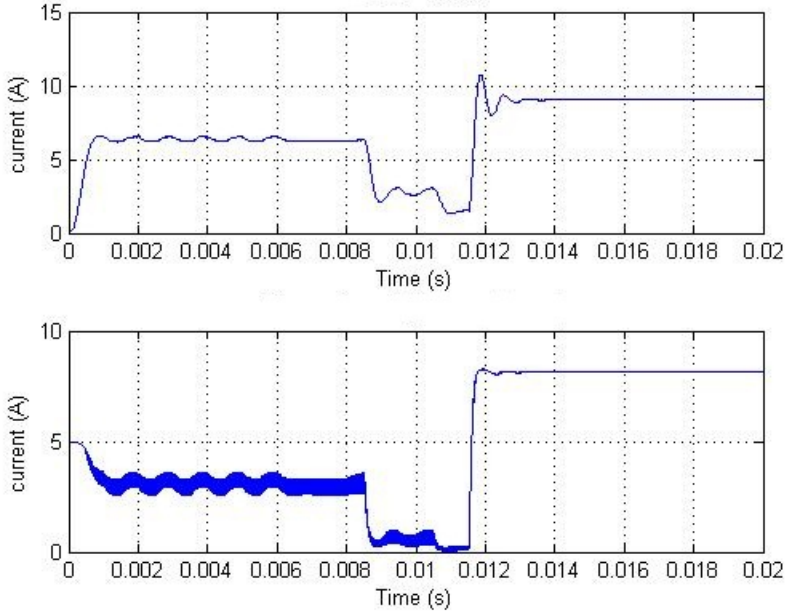

Figure 5.13: Perturb and Observe Algorithm Run 3. Source current (top) and output inductor (bottom) current versus time.

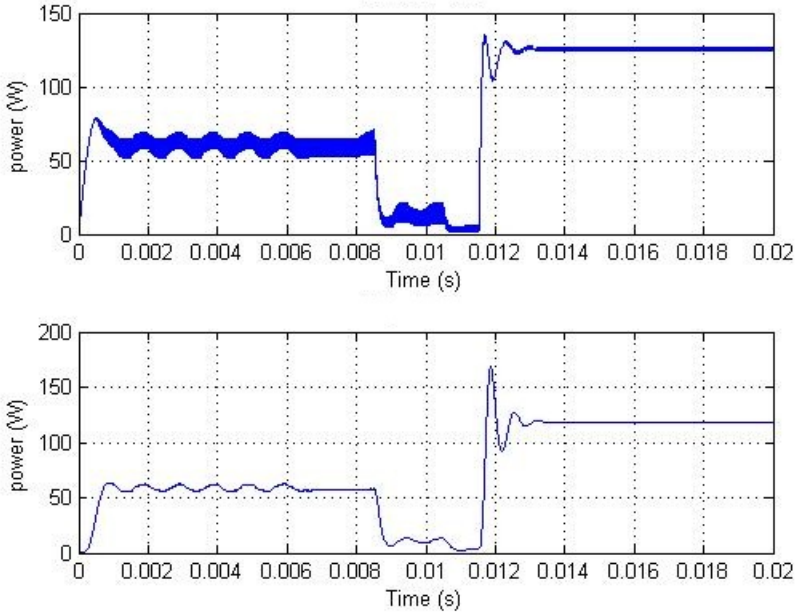

Figure 5.14: Perturb and Observe Algorithm Run 3. Source power (top) and output power (bottom) versus time.

5.4.4 Run 4: Constant D with Constant Irradiance.

This run was essentially a baseline test for the converter. The source and output voltage reach their peak after $0.001\,s$ with very little ripple in the output voltage as seen in Figure 5.16. The inductor current has a very small amount of ripple, which has a similar magnitude as the source current, as can be seen in Figure 5.17. The output power has a small dip at $0.001\,s$ due to the resonant nature of the output filter section of the buck converter. The response waveform has a normal damped response as seen in Figure 5.18. The efficiency as expected has the same profile as the output power due to the static nature of the input irradiance which is illustrated in Figure 5.15.

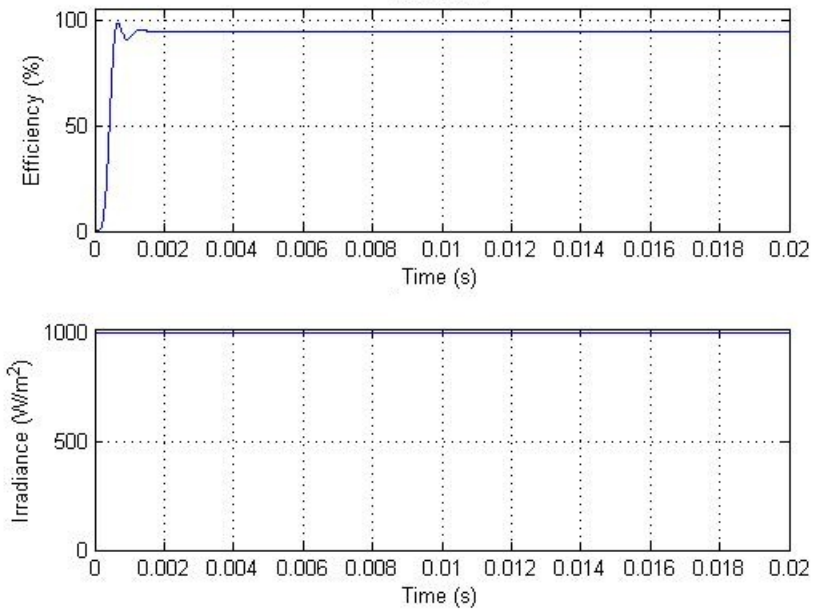

Figure 5.15: Constant Run 4. Converter efficiency (top) and irradiance (bottom) versus time.

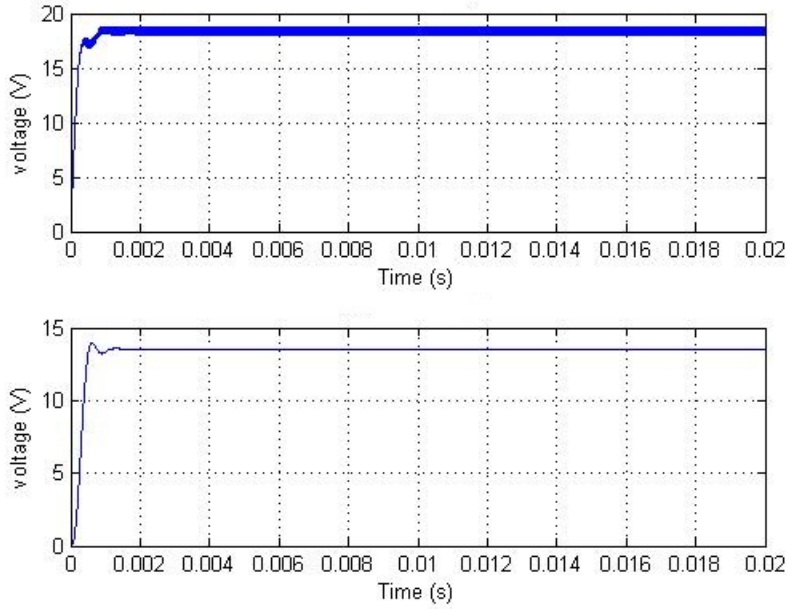

Figure 5.16: Constant Run 4. Source voltage (top) and output voltage (bottom) versus time.

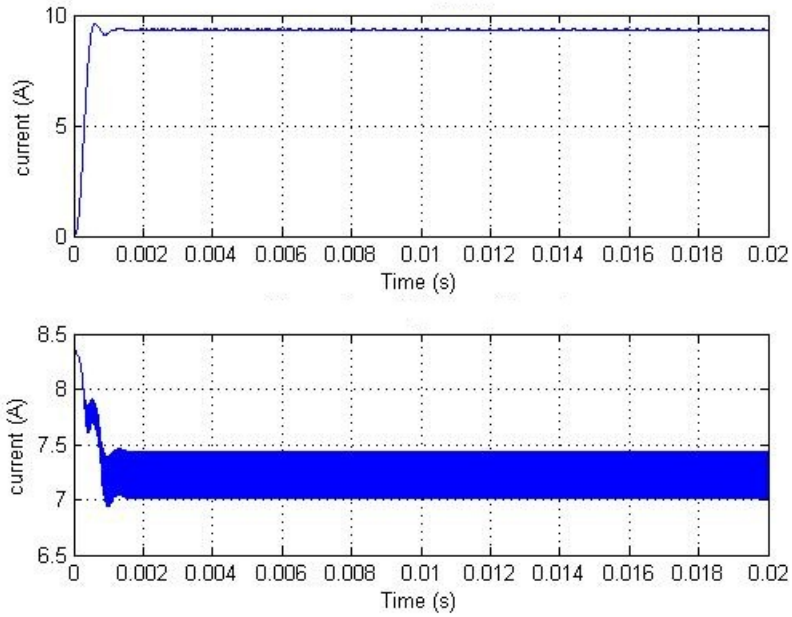

Figure 5.17: Constant Run 4. Source current (top) and output inductor current (bottom) versus time.

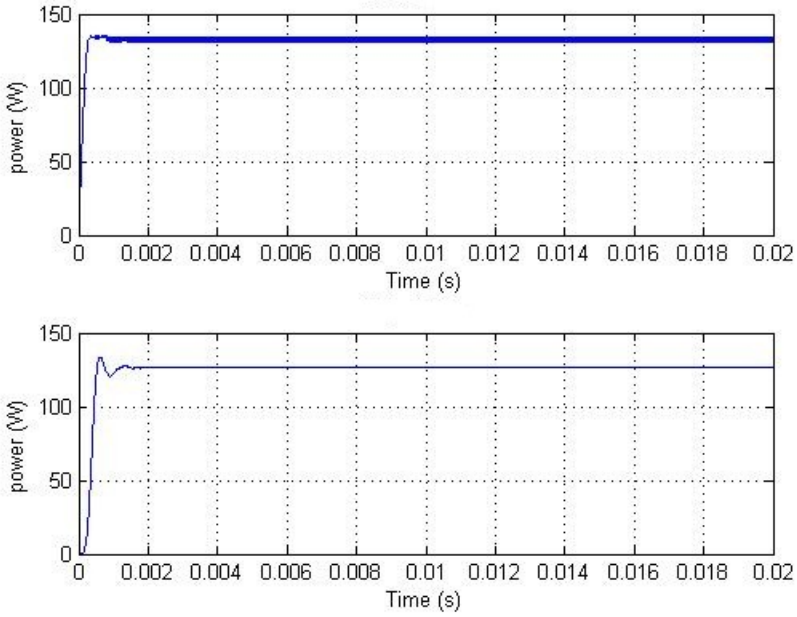

Figure 5.18: Constant Run 4. Source power (top) and output power (bottom) versus time.

5.4.5 Run 5: Constant D with Step in Irradiance.

This run used the constant D controller with a step in the input irradiance. The input and output voltage responded predictably to the change in irradiance; however, it was not tracking the MPP. The output voltage can be seen in Figure 5.20. The buck converter was operating at the MPP while under full irradiance. When the input irradiance reached $1000\,W/m^2$, the output power was $128\,W$. Since the solar array voltage was so low during the first $0.008\,s$, the output current also stayed at a lower than normal level, which can be seen in Figure 5.21. Since the normal output power at 60% irradiance is $81\,W$, the panels are operating far from the MPP by producing only $50\,W$, as seen in Figure 5.22. The converter efficiency was disrupted by the change in irradiance at $0.008\,s$, yet the converter efficiency remained fairly constant as seen in Figure 5.19.

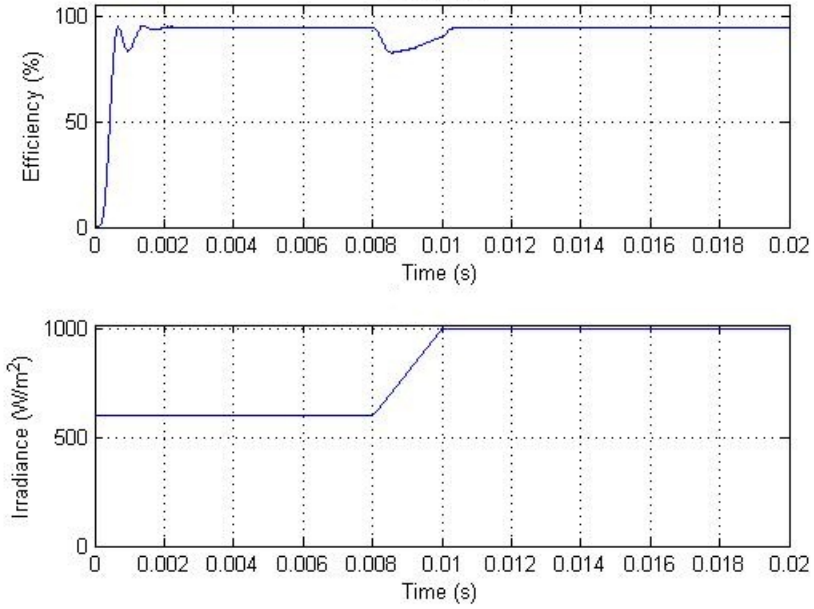

Figure 5.19: Constant Run 5. Converter efficiency (top) and irradiance (bottom) versus time.

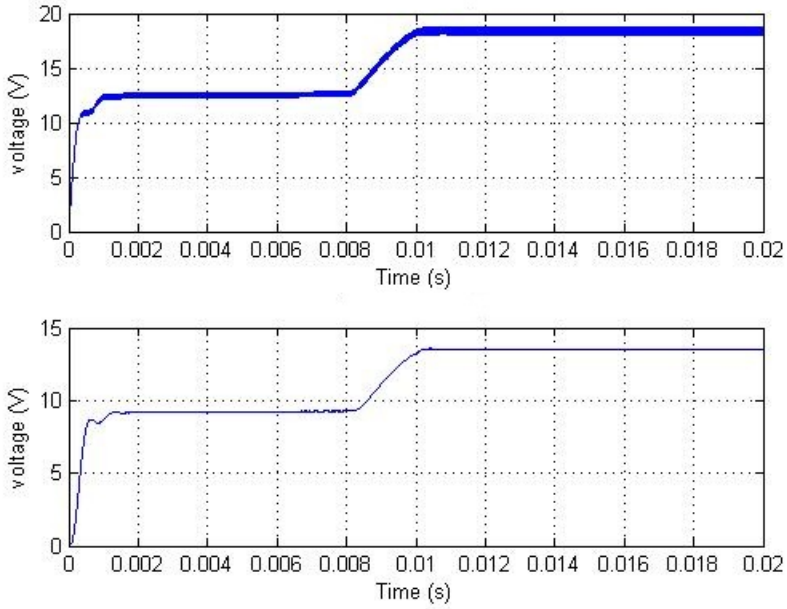

Figure 5.20: Constant Run 5. Source voltage (top) and output voltage (bottom) versus time.

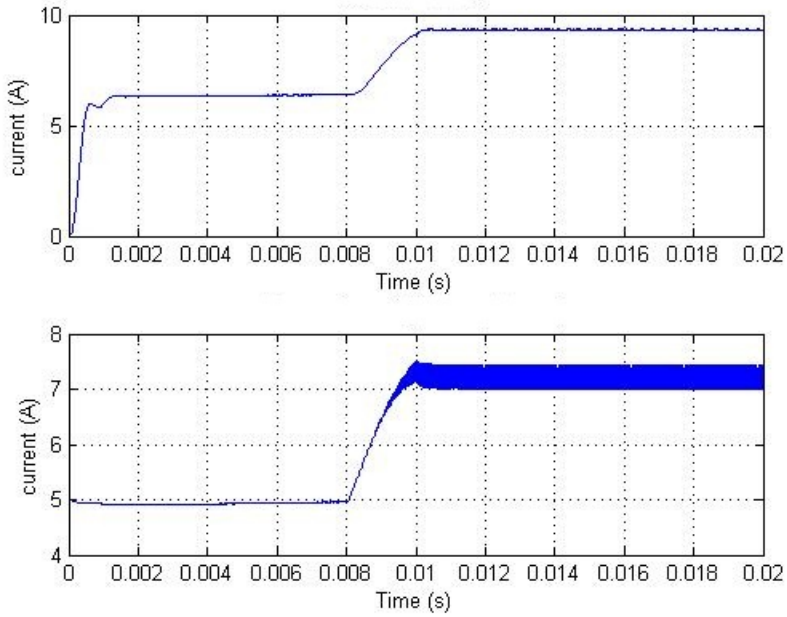

Figure 5.21: Constant Run 5. Source current (top) and output inductor current (bottom) versus time.

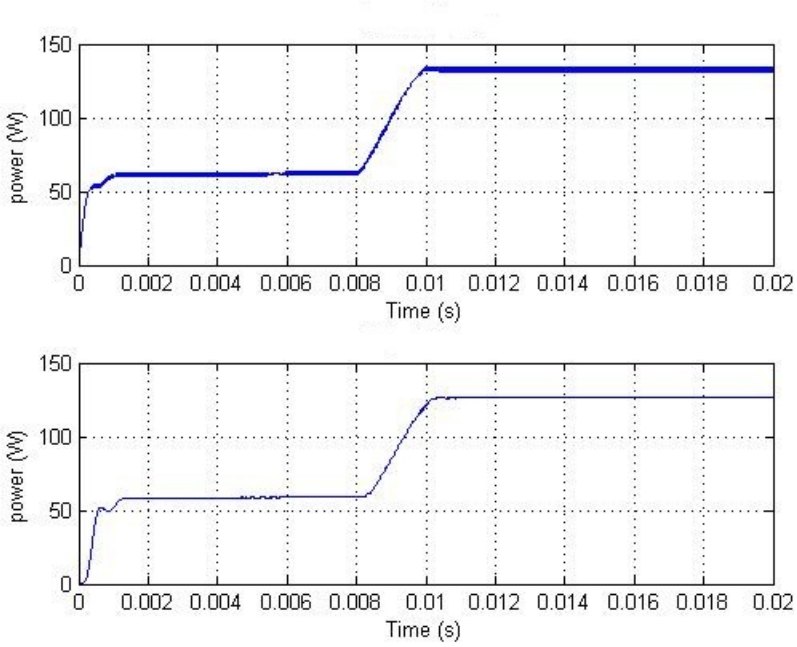

Figure 5.22: Constant Run 5. Source power (top) and output power (bottom) versus time.

5.4.6 Run 6: Constant D with Variable Irradiance.

With a variable irradiance, this controller performed the worst of all the algorithms. The source and output voltage profiles can be seen in Figure 5.24. At the lowest point in the irradiance, the output current dropped to $3.5\,A$. At this time the output voltage was $6\,V$. The output power was approximately $30\,W$ as seen in Figure 5.26. Luckily, the inductor current stayed very stable, seen in Figure 5.25, since the D was not changing. The converter efficiency was reasonably stable but overall very low as seen in Figure 5.23.

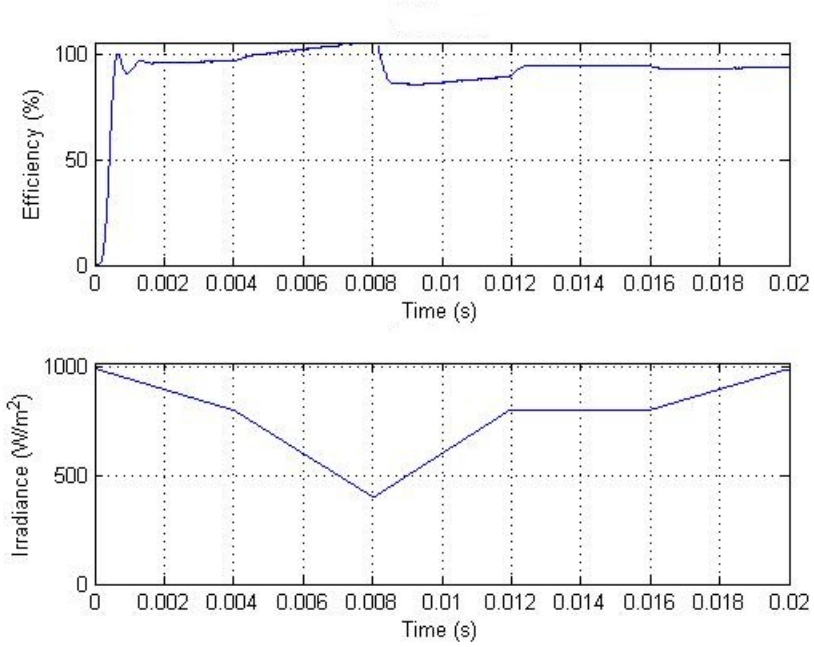

Figure 5.23: Constant Run 6. Converter efficiency (top) and irradiance (bottom) versus time.

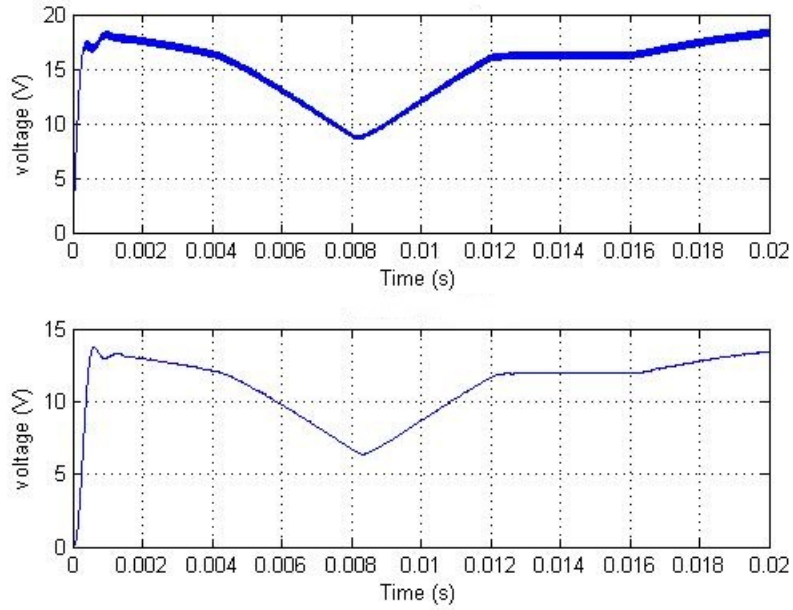

Figure 5.24: Constant Run 6. Source voltage (top) and output voltage (bottom) versus time.

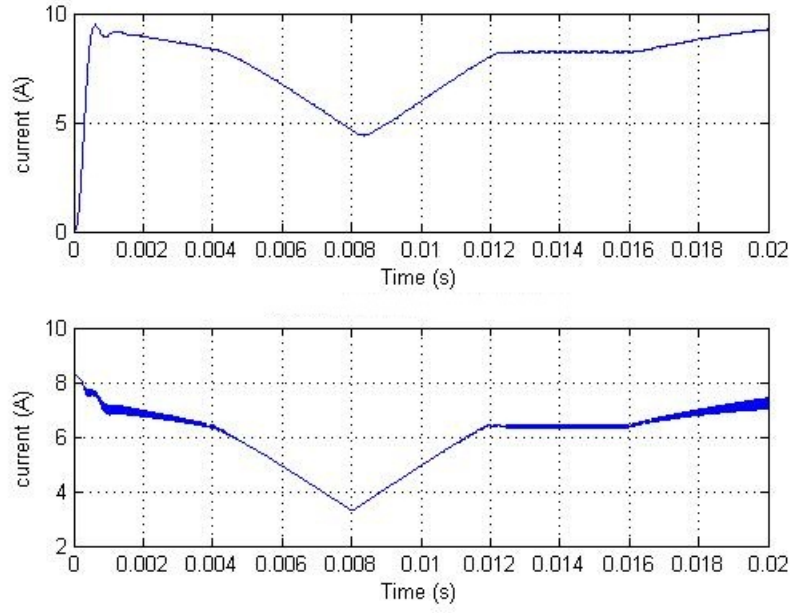

Figure 5.25: Constant Run 6. Source current (top) and output inductor current (bottom) versus time.

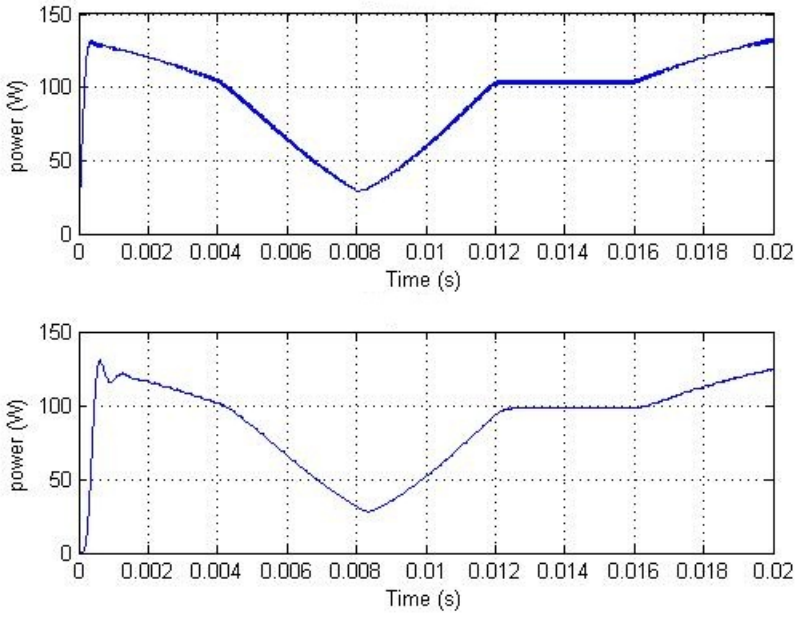

Figure 5.26: Constant Run 6. Source power (top) and output power (bottom) versus time.

5.4.7 Run 7: *InC* with Step in Irradiance.

This run used the *InC* algorithm, and the input irradiance has a step from $600\,W/m^2$ to $1000\,W/m^2$. While the irradiance is low, the source voltage tracks the *MPP* quite well and keeps the source and output power balanced as seen in Figure 5.28. There was a small amount of ripple in the source current as seen in Figure 5.29. Because of the current ripple, there is also ripple in the source power measurements. Luckily, the source ripple current does not transfer to the output current. The buck converter stabilizes the step in irradiance after $0.002\,s$ as seen in Figure 5.30. The converter efficiency does jump around quite a bit and has a rather large amount of ripple when it is stabilized as seen in Figure 5.27. This oscillation is due to the fast sampling rate set in the algorithm code.

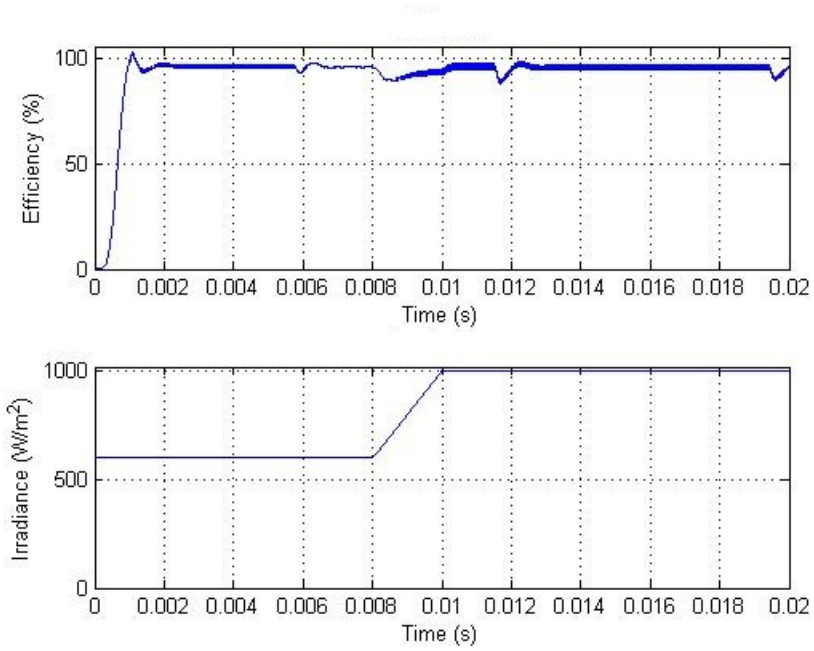

Figure 5.27: *InC* Run 7. Converter efficiency (top) and irradiance (bottom) versus time.

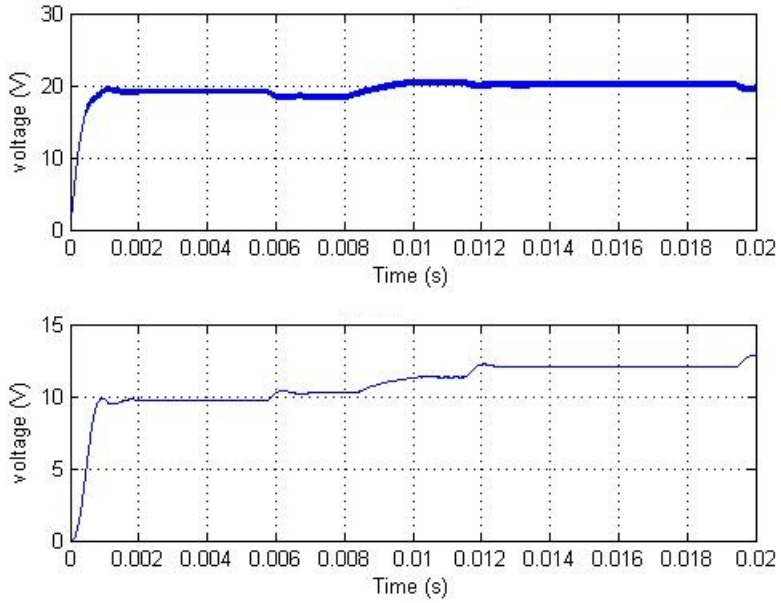

Figure 5.28: *InC* Run 7. Source voltage (top) and output voltage (bottom) versus time.

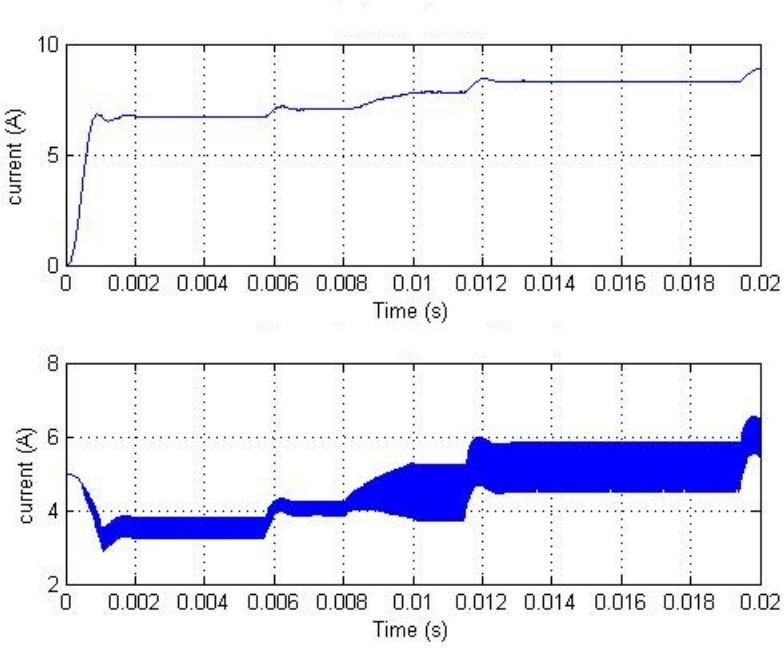

Figure 5.29: *InC* Run 7. Source current (top) and output inductor current (bottom) versus time.

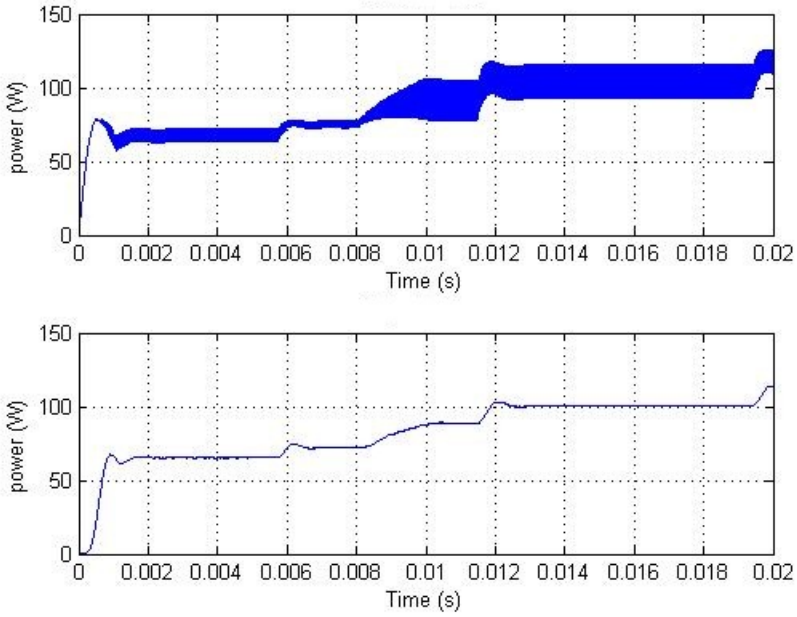

Figure 5.30: *InC* Run 7. Source power (top) and output power (bottom) versus time.

5.4.8 Run 8: *InC* with Variable Irradiance.

This run uses the *InC* algorithm with a variable input irradiance to the solar array. The source voltage and output voltage, seen in Figure 5.32, have a damped response after each change in the irradiance. The step size in D can be seen in Figure 5.33, where there is a stair step change in the current after $0.008\,s$. The power output of the converter tracked the *MPP* fairly well as seen in Figure 5.34. The largest oscillation occured in the calculation of efficiency. Since it was averaged across $0.001\,s$ there was a false surge in efficiency. The inductor and capacitor need time to return to the lower level of output power. This also caused the delay in the converter efficiency rising after the irradiance began increasing again as seen in Figure 5.31.

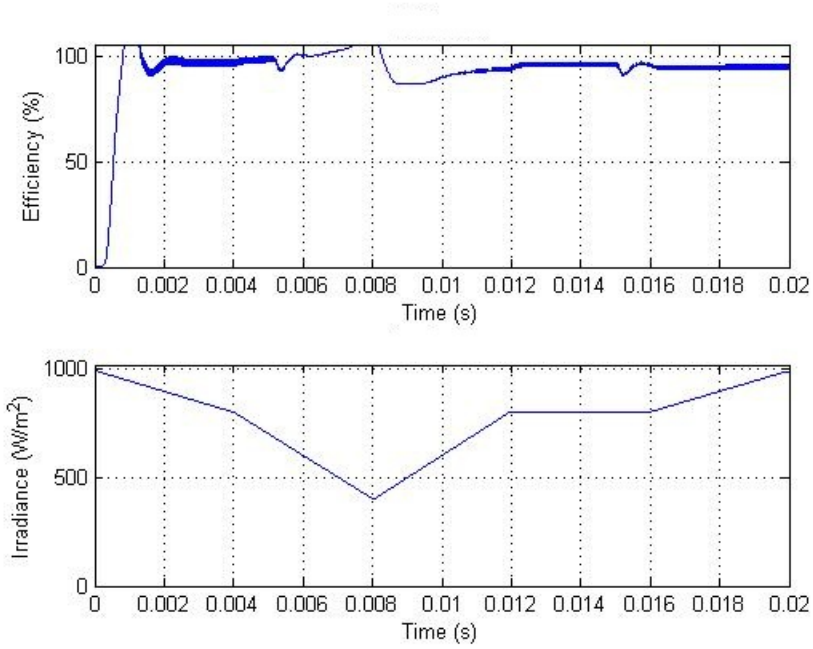

Figure 5.31: *InC* Run 8. Converter efficiency (top) and irradiance (bottom) versus time.

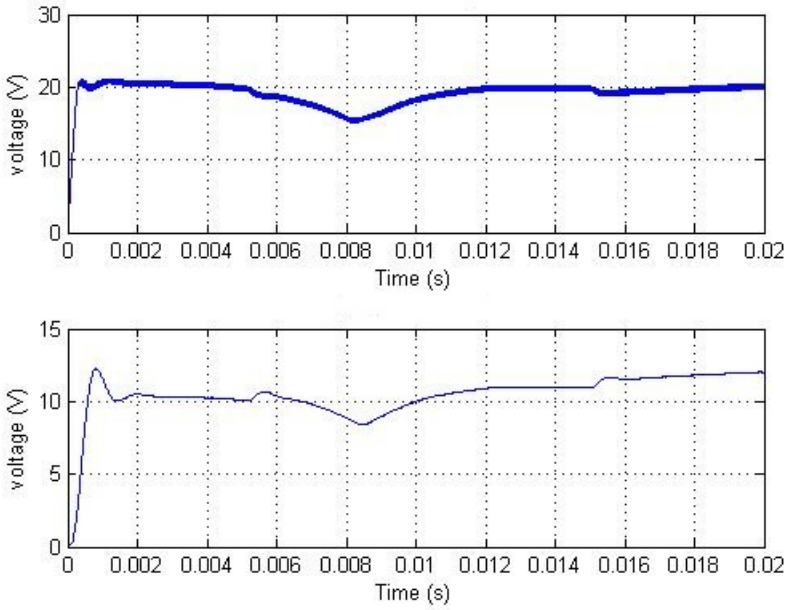

Figure 5.32: *InC* Run 8. Source voltage (top) and output voltage (bottom) versus time.

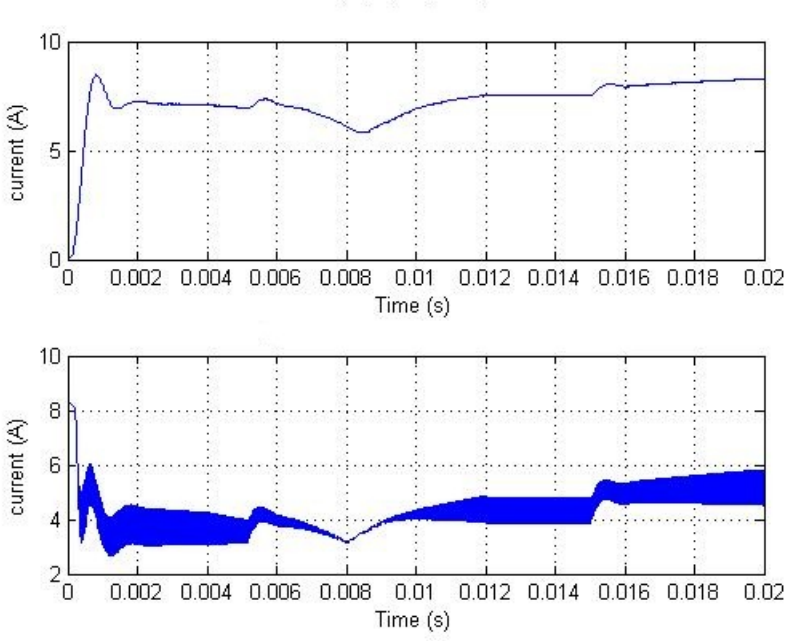

Figure 5.33: *InC* Run 8. Source current (top) and output inductor current (bottom) versus time.

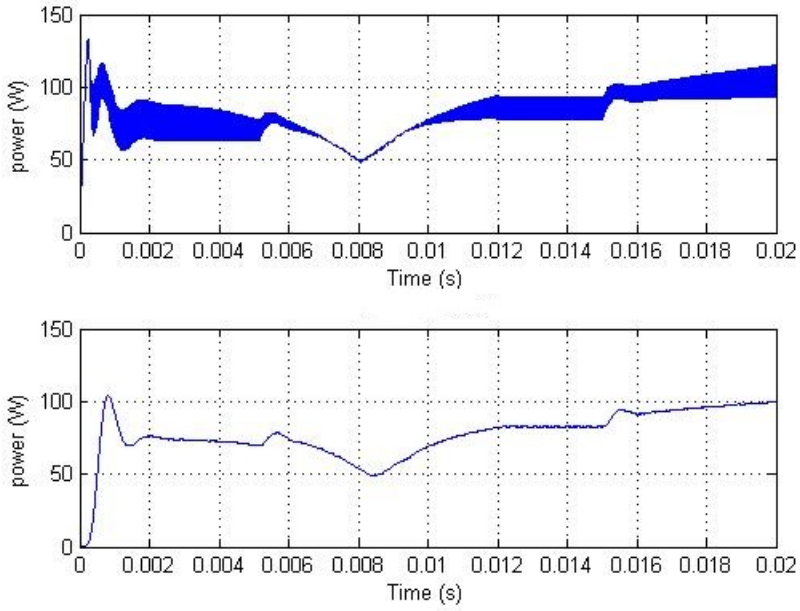

Figure 5.34: *InC* Run 8. Source power (top) and output power (bottom) versus time.

5.4.9 Run 9: *InC* with Constant Irradiance.

This run uses the *InC* algorithm with a constant input irradiance . The source voltage took longer to reach an acceptable level. The algorithm startes to track the *MPP* but due to the short length of the run, it does not actually reach the *MPP*. Although, it can be seen in Figure 5.36 that the algorithm was tracking in the correct direction and would reach the *MPP* in the next few iterations of the algorithm. The inductor current seen in Figure 5.37 has four jumps in D while tracking the *MPP*. With a final output power near $120\,W$, this algorithm takes a few iterations before converging to the *MPP* as seen in Figure 5.38. The converter efficiency is 97% for almost the entire run duration as seen in Figure 5.35.

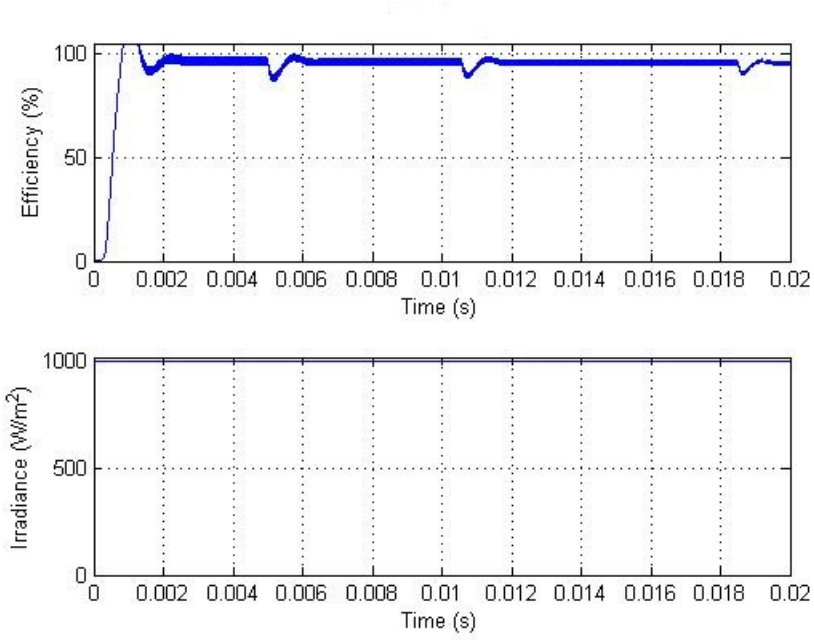

Figure 5.35: *InC* Run 9. Converter efficiency (top) and irradiance (bottom) versus time.

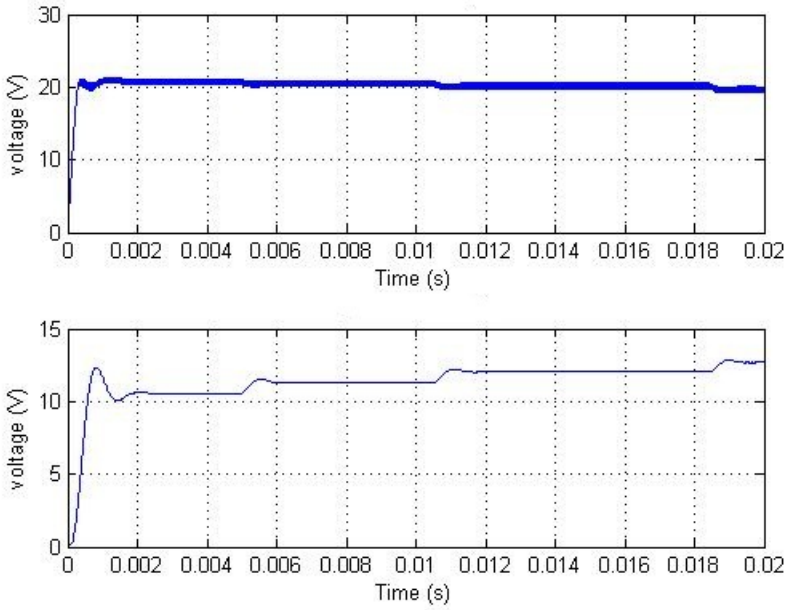

Figure 5.36: *InC* Run 9. Source voltage (top) and output voltage (bottom) versus time.

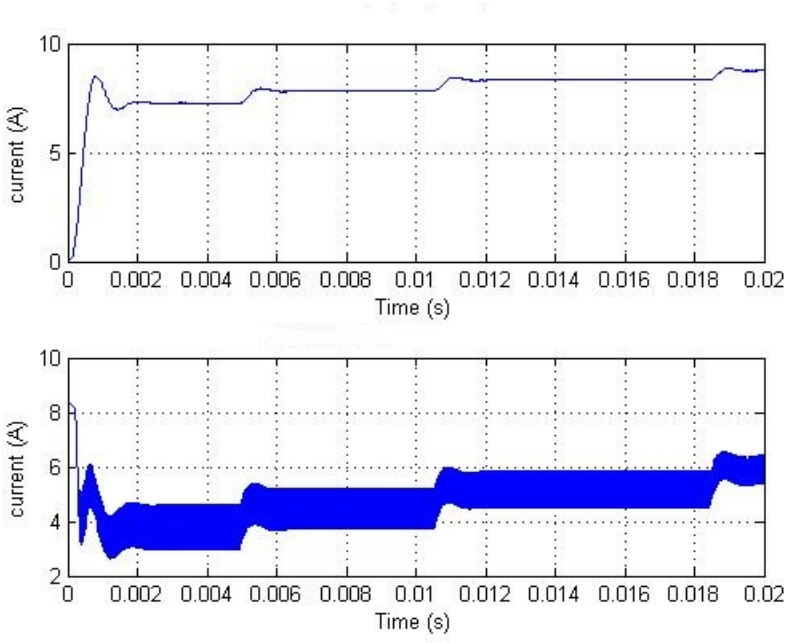

Figure 5.37: *InC* Run 9. Source current (top) and output inductor current (bottom) versus time.

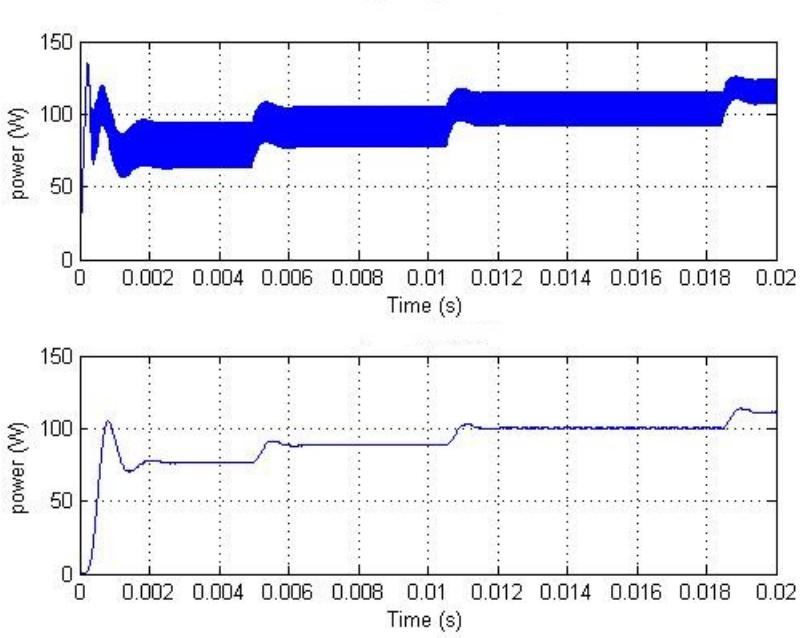

Figure 5.38: *InC* Run 9. Source power (top) and output power (bottom) versus time.

CHAPTER 6:

CONCLUSION AND FUTURE WORK

6.1 Conclusion

Overall the comparison of the *MPPT* algorithms was a worthwhile endeavor. Many of the problems inherit in this type of system can be solved or optimized to an acceptable level. This work could benefit future development solar powered *UAV*s.

In this thesis, the overall operation of the buck converter was covered. The different contributions of each component were discussed and how they each affected the output and functionality of the circuit. By optimizing the buck converter independent of the *MPPT* and the solar array, the efficiency of the converter was greater than 96% during steady-state operation. This makes the conversion from the solar array quite efficient and attractive.

The *MPPT* was discussed after the buck converter and greatly improved the tracking of the *MPP*. By having the ability to track the *MPP*, the *MPPT* algorithms further optimized the low efficiency solar array output. Since the solar array is the source of power to the system, any improvement in the ability to track the *MPP*, also greatly improves the overall system performance.

Next, the solar array model was discussed as well as designed around a single diode model. By modeling the solar array based on measured parameters, the output current and voltage were measured and used to drive the buck converter.

The actual data gathering runs were done in three parts. The first part included the *P&O* algorithm with constant $1000\,W/m^2$ irradiance, a step in irradiance from $600\,W/m^2$ to

$1000\,W/m^2$ at $0.08\,s$ to $0.01\,s$, and a random changing of irradiance to the solar array. Next, the constant D controller was tested with the same three input signals. The constant D was tested as the reference for comparison with the other algorithms. Finally, the *InC* algorithm was tested; although, the tuning of the parameters for this algorithm was the most difficult. The algorithm leads to either a very fast response to transients or undershoots the *MPP*. Because of the difficulty optimizing and the amount of time required to actually run each test, the *InC* algorithm was not optimized to match the performance of the *P&O* algorithm.

By including a two-stage change in D, the *P&O* algorithm was further optimized. This innovation was necessary in order to converge quickly to the *MPP* yet still have fine granularity when approaching the *MPP*. This addition was not very difficult to implement and overall provided very fast tracking and convergence to the *MPP*. In the Appendix, the code used for this algorithm is provided. It can be seen that with a multistage *MPPT*, the overall speed of the system will remain fast and track the *MPP* well.

Overall, the outcome of the *P&O* algorithm tests were quite good. Since the algorithm can be optimized to meet certain timing requirements, it responded faster and performed better than the *InC* algorithm. This can only be accounted for due to the complexities of the *InC* algorithm computations and speed of operation. Due to the difficulty in optimizing the *InC* algorithm, the results from those runs do not accurately give the optimal operation of the algorithm. Given more time to properly optimize the ΔD, the algorithm should have tracked the *MPP* quicker and with more certainty than the *P&O* algorithm.

6.2 Future Work

There are a few optimizations that were not integrated into the thesis but would be valuable to include.

6.2.1 *UAV* Flight Endurance

In the modern *UAV*, most onboard components are run from a battery. Similar to satellites, *UAV*s require battery power to be replenished at some point. If all of the power for the system comes from the battery, it seems logical to try and extend the range and time the *UAV* will be on a mission. In order to accomplish this, thin film solar panels can be laminated to the surface of the wings of these *UAV*s and used to deliver power to the batteries while in flight. With the inclusion of an *MPPT*, the solar panels on the wing will be optimized for when the *UAV* turns to a non-optimal power generation angle.

6.2.2 Second Stage Constant Voltage Output

In order to actually use the output power from the *MPPT*, a second stage constant voltage controller would also be necessary to provide the power required to charge a battery system. This battery system would then have all the equipment connected to that so the voltage would be quite stable at the equipment.

Without this extra controller the battery charger attached to the buck converter would not have a high enough voltage if the irradiance dropped too low. Depending on the amount of light and the configuration of the solar panels, a buck-boost converter might be better suited for this application.

6.2.3 Test *MPPT* on Real Hardware

A proof-of-concept for this simulation would be to use real hardware to control a buck converter. Unfortunately, we did not have the required time to change the laboratory setup and run the algorithm on real hardware.

6.2.4 More Complex Variable ΔD Modulation

Even more advanced than the two stage *P&O D* modulation would be to have the ΔD be variable based on a lookup table of the *MPP*. This would have an adjustable gain which was adjusted by the distance to the *MPP*. The two-stage *P&O* algorithm implemented in this thesis is quite similar to automatic sliding ΔD modulation except that it does not adapt to changing parameters as well.

Appendix: DATASHEET & MATLAB CODE

Datasheet for Kyocera KD135GX-LP

MODEL
KD135GX-LP

THE NEW VALUE FRONTIER

KYOCERA

KD135GX-LP

HIGH EFFICIENCY MULTICRYSTAL
PHOTOVOLTAIC MODULE

UL LISTED

HIGHLIGHTS OF KYOCERA PHOTOVOLTAIC MODULES

Kyocera's advanced cell processing technology and automated production facilities produce a highly efficient multicrystal photovoltaic module.
The conversion efficiency of the Kyocera solar cell is over 16%.
These cells are encapsulated between a tempered glass cover and a pottant with back sheet to provide efficient protection from the severest environmental conditions.
The entire laminate is installed in an anodized aluminum frame to provide structural strength and ease of installation.
Equipped with plug-in connectors.

APPLICATIONS

KD135GX-LP is ideal for grid tie system applications.

- Residential roof top systems
- Large commercial grid tie systems
- Water Pumping systems
- High Voltage stand alone systems
- etc.

QUALIFICATIONS

- **MODULE** : UL1703 listed
- **FACTORY** : ISO9001 and ISO 14001

QUALITY ASSURANCE

Kyocera multicrystal photovoltaic modules have passed the following tests.

- Thermal cycling test
- Thermal shock test
- Thermal / Freezing and high humidity cycling test
- Electrical isolation test
- Hail impact test
- Mechanical, wind and twist loading test
- Salt mist test
- Light and water-exposure test
- Field exposure test

LIMITED WARRANTY

※1 year limited warranty on material and workmanship
※20 years limited warranty on power output: For detail, please refer to "category IV" in Warranty issued by Kyocera

(Long term output warranty shall warrant if PV Module(s) exhibits power output of less than 90% of the original minimum rated power specified at the time of sale within 10 years and less than 80% within 20 years after the date of sale to the Customer. The power output values shall be those measured under Kyocera's standard measurement conditions. Regarding the warranty conditions in detail, please refer to Warranty issued by Kyocera)

ELECTRICAL CHARACTERISTICS

Current-Voltage characteristics of Photovoltaic Module KD135GX-LP at various cell temperatures

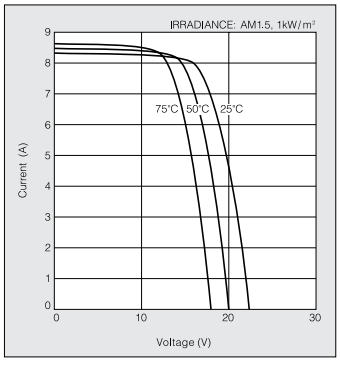

Current-Voltage characteristics of Photovoltaic Module KD135GX-LP at various irradiance levels

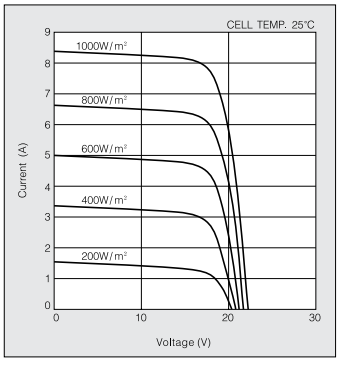

Physical Specifications

Unit : mm (in.)

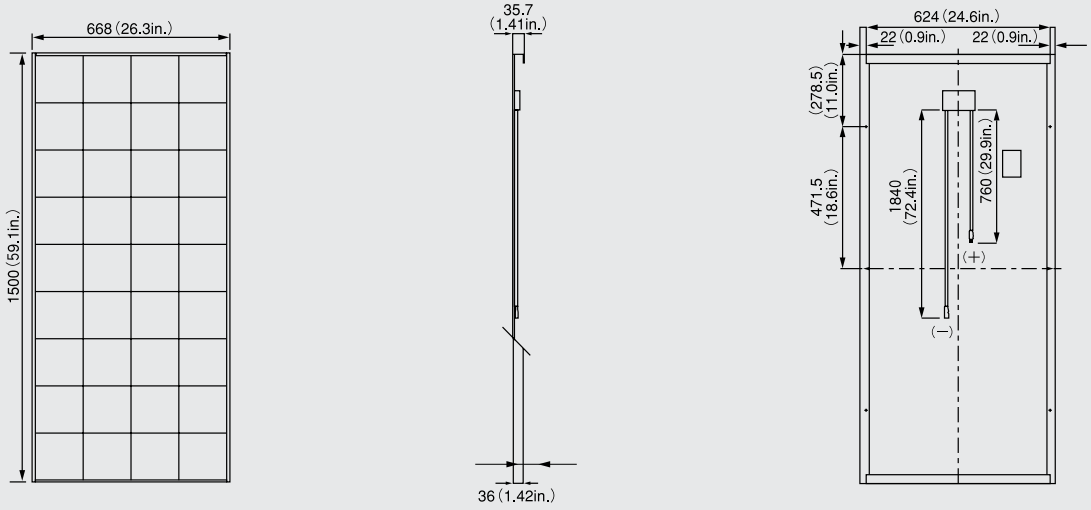

Specifications

Electrical Performance under Standard Test Conditions (*STC)	
Maximum Power (Pmax)	135W (+5%/−5%)
Maximum Power Voltage (Vmpp)	17.7V
Maximum Power Current (Impp)	7.63A
Open Circuit Voltage (Voc)	22.1V
Short Circuit Current (Isc)	8.37A
Max System Voltage	600V
Temperature Coefficient of Voc	−.080 V/℃
Temperature Coefficient of Isc	5.02×10^{-3} A/℃

*STC : Irradiance 1000W/m², AM1.5 spectrum, cell temperature 25℃

Electrical Performance at 800W/m², *NOCT, AM1.5	
Maximum Power (Pmax)	95W
Maximum Power Voltage (Vmpp)	15.6V
Maximum Power Current (Impp)	6.10A
Open Circuit Voltage (Voc)	19.9V
Short Circuit Current (Isc)	6.82A

*NOCT (Nominal Operating Cell Temperature) : 49℃

Cells	
Number per Module	36

Module Characteristics	
Length × Width × Depth	1500mm(59.1in)×668mm(26.3in)×36mm(1.4in)
Weight	13.0kg(28.7lbs.)
Cable	(+)760mm(29.9in),(-)1840mm(72.4in)

Junction Box Characteristics	
Length × Width × Depth	100mm(3.9in)×108mm(4.3in)×15mm(0.6in)
IP Code	IP65

Others	
*Operating Temperature	−40℃～90℃
Maximum Fuse	15A

*This temperature is based on cell temperature.

Please contact our office for further information

KYOCERA

KYOCERA Corporation

■ KYOCERA Corporation Headquarters
CORPORATE SOLAR ENERGY DIVISION
6 Takeda Tobadono-cho
Fushimi-ku, Kyoto
612-8501, Japan
TEL:(81)75-604-3476 FAX:(81)75-604-3475
http://www.kyocera.com/

● KYOCERA Solar, Inc.
7812 East Acoma Drive
Scottsdale, AZ 85260, USA
TEL:(1)480-948-8003 or (800)223-9580 FAX:(1)480-483-6431
http://www.kyocerasolar.com/

● KYOCERA Solar do Brasil Ltda.
Av. Guignard 661, Loja A
22790-200, Recreio dos Bandeirantes, Rio de Janeiro, Brazil
TEL:(55)21-2437-8525 FAX:(55)21-2437-2338
http://www.kyocerasolar.com.br/

● KYOCERA Solar Pty Ltd.
Level 3, 6-10 Talavera Road, North Ryde
N.S.W. 2113, Australia
TEL:(61)2-9870-3948 FAX:(61)2-9888-9588
http://www.kyocerasolar.com.au/

● KYOCERA Fineceramics GmbH
Fritz-Muller-Strasse 107, 73730 Esslingen Germany
TEL:(49)711-93934-999 FAX:(49)711-93934-950
http://www.kyocerasolar.de/
solar@kyocera.de

● KYOCERA Asia Pacific Pte. Ltd.
298 Tiong Bahru Road, #13-03/05
Central Plaza, Singapore 168730
TEL:(65)6271-0500 FAX:(65)6271-0600

● Kyocera Asia Pacific Ltd.
Room 801-802, Tower 1, South Seas Centre,
75 Mody Road, Tsimshatsui East, Kowloon, Hong Kong
TEL:(852)2723-7183 FAX:(852)2724-4501

● KYOCERA Asia Pacific Pte. Ltd., Taipei Office
10F, No. 66, Nanking West Road, Taipei, Taiwan
TEL:(886) 2-2555-3609 FAX:(886)2-2559-4131

● KYOCERA (Tianjin) Sales & Trading Corp.
(Beijing Office)Room 2107, Beijing Huabin International Building,
No.8 Yong An Dong Li, Jian Guo Men Wai Road, Chao Yang District,
Beijing, 100022, China
TEL:(86)10-8528-8838 FAX:(86)10-8528-8839
http://www.kyocera.com.cn/

● KYOCERA Korea Co., Ltd.
Diplomatic Center Room #406, 1376-1,
Seocho-2Dong, Seocho-Ku,Seoul, 137-072, Korea
TEL:(82)2-3463-3538 FAX:(82)2-3463-3539
http://www.kyocera.co.kr/

'P&O'

```
function Duty  = MPPT(V,I)
persistent PowerNew PowerOld DifferenceOfPower d DutyDifference n i OldV;
if isempty(V)
    V=20;
end
if isempty(I)
    I=0;
end
if isempty(OldV)
    OldV=0;
end
if isempty(PowerOld)
    PowerOld=0;
end
if isempty(PowerNew)
    PowerNew=0;
end
if isempty(DifferenceOfPower)
    DifferenceOfPower=0;
end
if isempty(d)
    d=1;
end
if isempty(DutyDifference)
```

```
    DutyDifference=0;
end
if isempty(n)
    n=500;
end
if isempty(i)
    i=1;
end


  PowerOld = PowerNew;
  PowerNew=V*I;
  DifferenceOfPower = PowerNew-PowerOld;
if( i > n )
    i = 1;
    if (DifferenceOfPower > .01)
        if(V > OldV)
            if(DifferenceOfPower > 1) %if power>1
                DutyDifference=.75;
                d=d+DutyDifference;
            else %if .01<power<1
                DutyDifference=.025;
                d=d+DutyDifference;
            end
        else %V<OldV
            if(DifferenceOfPower > 1)
                DutyDifference=-.75;
```

```
            d=d+DutyDifference;
        else %if .01<power<1
            DutyDifference=-.025;
            d=d+DutyDifference;
        end
    end
else
    if(DifferenceOfPower < -.01)
        if(V<OldV)
            if(DifferenceOfPower <-1)
                DutyDifference=-.75;
                d=d+DutyDifference;
            else %if -.01<power <-1
                DutyDifference=-.025;
                d=d+DutyDifference;
            end
        else %V>OldV
            if(DifferenceOfPower < -1)
                DutyDifference=.75;
                d=d+DutyDifference;
            else
                DutyDifference=.025;
                d=d+DutyDifference;
            end
        end
    else
```

```
            DutyDifference=0;
        end
    end

else
    i=i+1;
end

Duty=d/(d+1);
%keep spikes in duty cycle under control.
if (Duty >.9)
    Duty=.9;
else
    if(Duty < .1)
        Duty = .1;
    end
end

OldV=V;
end
```

'InC'

```
function Duty  = MPPTIC(V,I)
persistent DeltaVoltage DeltaCurrent d DutyDifference n i OldV OldI;
if isempty(V)
```

```
    V=20;
end
if isempty(I)
    I=0;
end
if isempty(OldV)
    OldV=0;
end
if isempty(OldI)
    OldI=0;
end
if isempty(DeltaVoltage)
    DeltaVoltage=0;
end
if isempty(DeltaCurrent)
    DeltaCurrent=0;
end


if isempty(d)
    d=1;
end
if isempty(DutyDifference)
    DutyDifference=0;
end
if isempty(n)
    n=1;
```

```
end
if isempty(i)
    i=1;
end


    DeltaVoltage = V-OldV;
    DeltaCurrent = I-OldI;
%start main loop
if( i > n )
    i = 1;
    if (abs(DeltaVoltage) <= .01)
        if(abs(DeltaCurrent) <= .01)
            %No Change;
        else
            if(DeltaCurrent > 0)
                d=d+.0001;
            else
                d=d-.0001;
            end
        end
    else
        if(abs((DeltaCurrent/DeltaVoltage)+I/V)  < .001)
            %no change
        else
            if((DeltaCurrent/DeltaVoltage) < -I/V)
                d=d+.0001;
```

```
            else
                d=d-.0001;
            end
        end
    end

else
    i=i+1;
end



Duty=d/(d+1);
if (Duty >.9)
    Duty=.9;
else
    if(Duty < .1)
        Duty = .1;
    end
end
OldV=V;
OldI=I;
end
```

REFERENCES

[1] E. Weston, "Art of utilizing solar radiant energy," September 1888.

[2] A. Einstein, "Concerning an heuristic point of view toward the emission and transformation of light," *American Journal of Physics*, vol. 33, no. 5, 1965.

[3] D. M. Chapin, C. S. Fuller, and G. L. Pearson, "A new silicon pn junction photocell for converting solar radiation into electrical power," *Journal of Applied Physics*, vol. 25, p. 676, 1954.

[4] "Missions - tiros - nasa science." `http://science.nasa.gov/missions/tiros/`, Nov 2012.

[5] "The mission of soyuz-1." `http://www.russianspaceweb.com/soyuz1.html`, Nov 2012.

[6] "The institute of energy conversion: The first twenty-five years: 1972-1997." `http://www.udel.edu/iec/history.html`, Nov 2012.

[7] "University of delaware-led team sets solar cell record, joins dupont on $100 million project.." `http://www.renewableenergyworld.com/rea/news/article/2007/07/from-40-7-to-42-8-solar-cell-efficiency-49483`, Nov 2012.

[8] "Best research cell efficiencies." `http://en.wikipedia.org/wiki/File:PVeff(rev100414).png`, April 2010.

[9] N. Mohan, *Power Electronics: Converters, Applications, and Design*. Wiley, 2002.

[10] W. Hurd, "Applicaion of copper indium gallium diselenide photovoltaic cells to extend the endurance and capabilities of unmanned aerial vehicles," Master's thesis, Naval Postgraduate School, Monterey, CA, 2009.

[11] J. Coba, "Design of solar powered airplanes for continuous flight," Master's thesis, Naval Postgraduate School, Monterey, CA, 2010.

[12] S. S. Mohammed, "Modeling and simulation of photovoltaic module using matlab/simulink," *International Journal of CHemial and Environmental Engineering*, vol. 2, no. 5, pp. 350–355, 2011.

[13] I. Glasner and J. Appelbaum, "Advantage of boost vs buck topology for maximum power point tracker in photovoltaic systems," pp. 355–358, 1996.

[14] A. P. K. Yadav, S. Thirumaliah, and G. Haritha, "Comparison of mppt algorithms for dc-dc converters based pv systems," *International Journal of Advanced Research in Electrical, Electronics, and Instrumentation Enginering*, vol. 1, no. 1, pp. 18–23, 2012.

[15] Z. Liang and R. Huang, A. Q.and Guo, "High efficiency switched capacitor buck-boost converter for pv application," pp. 1951–1958, 2012.

[16] G. Barca, A. Moschetto, C. Sapuppo, G. M. Tina, R. Giusto, and A. D. Grasso, "A novel mppt charge regulator for photovoltaic stand-alone telecommunication system," pp. 235–238, 2008.

[17] M. Azab, "Improved circuit model of photovoltaic array," *International journal of electrical power and energy systems engineering*, vol. 2, no. 3, pp. 185–188, 2009.

[18] D. P. Hohm and M. E. Ropp, "Comparative study of maximum power point tracking algorithms," *Progress in Photovoltaics: Research and Applications*, vol. 11, pp. 47–62, 2003.

[19] S. Gomathy, S. Saravanan, and D. S. Thangavel, "Design and implimentation of maximum power point tracking algorithm for a standalone pv system," *International journal of scientific and engineering research*, vol. 3, no. 3, 2012.

[20] V. A. Chaudhari, "Automatic peak power tracker for solar pv modules using dspacer software.," Master's thesis, MAULANA AZAD NATIONAL INSTITUTE OF TECHNOLOGY, Deemed University, Bhopal, India, 2005.

[21] V. Salas, E. Olías, A. Barrado, and A. Lázaro, "Review of the maximum power point tracking algorithms for stand-alone photovoltaic systems," *Solar Energy Materials and Solar Cells*, vol. 90, pp. 1555–1578, July 2006.

THIS PAGE INTENTIONALLY LEFT BLANK

INITIAL DISTRIBUTION LIST

1. Defense Technical Information Center
   Ft. Belvoir, Virginia
2. Dudly Knox Library
   Naval Postgraduate School
   Monterey, California
3. Clark Robertson, ECE Chair
   Naval Postgraduate School
   Monterey, California
4. Robert Ashton, Thesis Advisor
   Naval Postgraduate School
   Monterey, California
5. Vladimir Dobrokhodov, Second Reader
   Naval Postgraduate School
   Monterey, California
6. Jeff Wurz, Thesis Author
   Naval Postgraduate School
   Monterey, California